A New Efficient Algorithm for Volume-Preserving Parameterizations of Genus-One 3-Manifolds*

Mei-Heng Yeh†, Tiexiang Li‡, Wen-Wei Lin§, and Shing-Tung Yau¶

Abstract. Parameterizations of manifolds are widely applied to the fields of numerical partial differential equations and computer graphics. To this end, in recent years several efficient and reliable numerical algorithms have been developed by different research groups for the computation of triangular and tetrahedral mesh parameterizations. However, it is still challenging when the topology of manifolds is nontrivial, e.g., the 3-manifold of a topological solid torus. In this paper, we propose a novel volumetric stretch energy minimization algorithm for volume-preserving parameterizations of toroidal polyhedra with a single boundary being mapped to a standard torus. In addition, the algorithm can also be used to compute the equiareal mapping between a genus-one closed surface and the standard torus. Numerical experiments indicate that the developed algorithm is effective and performs well on the bijectivity of the mapping. Applications on manifold registrations and partitions are demonstrated to show the robustness of our algorithms.

Key words. volumetric stretch energy, energy minimization, volume-preserving, toroidal polyhedra

AMS subject classifications. 15B48, 52C26, 65F05, 68U05, 65D18

1. Introduction.

A 3-manifold refers to a 3-dimensional topological space that each point of the 3-manifold has a neighborhood being homeomorphic to a subset of $\mathbb{R}^3$. In recent years, 3D imaging technologies, such as the magnetic resonance image (MRI) and the computed tomography (CT) scan, have successfully been developed in real-world applications. These issues raise the importance of 3-manifold parameterizations. A 3-manifold parameterization represents a bijective mapping between the 3-manifold and the 3-dimensional domain with a simple canonical shape. The mapping can be used to produce a canonical coordinate system on the 3-manifold for simplifying problems arising from complicated geometry processing and computer graphics. However, the bijectivity of the volumetric mapping is, in general, very difficult to be guaranteed due to that the convex combination mapping in 3D space is not necessary to be bijective, an elegant counterexample can be found in [20]. Therefore, it points out that conformal (angle-preserving) mappings between 3-manifolds generally do not exist. Yet, volumetric mappings with a small angular distortion are frequently used. Paillé and Poulin

*Submitted to the editors DATE.

Funding: The work of M.-H. Yueh was partially supported by the Ministry of Science and Technology (MOST) 107-2115-M-003-012-MY2. The work of T. Li was supported in parts by the National Natural Science Foundation of China (NSFC) 11971105. The work of W.-W. Lin was partially supported by the MOST 106-2628-M-009-004-. The work of the authors was partially supported by the MOST, the National Center for Theoretical Sciences (NCTS), the ST Yau Center in Taiwan, the Shing-Tung Yau Center at Southeast University, the Nanjing Center for Applied Mathematics (NCAM), and the Center of Mathematical Sciences and Applications (CMSA) at Harvard University.

†Department of Mathematics, National Taiwan Normal University, Taipei, Taiwan (yue@ntnu.edu.tw).

‡School of Mathematics, Southeast University, Nanjing, China (txli@seu.edu.cn).

§Department of Applied Mathematics, National Chiao Tung University, Hsinchu, Taiwan (wwlin@math.nctu.edu.tw).

¶Department of Mathematics, Harvard University, Cambridge, USA (yau@math.harvard.edu).

[32], as well as Chern et al. [8] proposed conformal-based volumetric mapping algorithms by applying the Cauchy-Riemann equation to a canonical orthogonal plane in $\mathbb{R}^3$ with a low shear distortion. Based on the dihedral angle representation, Paillé et al. [33] proposed a spectral method for the computation of the locally injective mapping of tetrahedral meshes. With bounded constraints of distortion, Kovalsky et al. [29, 30] developed algorithms to deform a given volumetric mapping into a bijective one. By minimizing the stretch-distortion energy with balancing between angle and volume distortions, Jin et al. [28] developed an algorithm for the computation of the volumetric parameterization. Based on minimizing a linear combination of local isometric distortion measures [36], and the quasi-conformal homeomorphism, respectively, Rabinovic et al. [34] and Naitsat et al. [31] proposed deformation algorithms for volumetric meshes. The above algorithms are, in general, not volume-preserving, but have mainly been developed for the computation of bijective volumetric mappings of 3-manifolds by minimizing angular distortions such that the quality on local shapes of tetrahedral meshes is well-preserved.

Additionally, only a few of the existing algorithms consider finding volume-preserving parameterizations by minimizing the volume distortion for prescribed tetrahedral meshes. Based on the discrete optimal mass transportation (OMT) [21], Su et al. [37] first proposed an algorithm to realize the volume-preserving parameterization between a genus-zero 3-manifold and the solid unit ball $\mathbb{B}^3$. However, it is somewhat time-consuming, especially, when the high-resolution mesh data, e.g., the volume-mesh of 290K tetrahedrons (human brain), is considered. Very recently, based on minimizing the volumetric stretch energy, Yueh et al. [45] developed a significantly efficient volume-preserving parameterization between a genus-zero 3-manifold and $\mathbb{B}^3$ to improve the convergence from 15 hours to 157.8 sec. for the above example.

Now we go back to the discussion of closed surfaces. In the past ten years, several numerical algorithms based on minimizing the distortion of angles [11, 12, 9, 46] or area [49, 38, 10, 47] or balancing between them [43, 34, 35] have been widely developed to find the angle-preserving (conformal/quasi-conformal) and area-preserving (authalic/equiareal) parameterizations, respectively, to a sphere $\mathbb{S}^2$ or a disk $\mathbb{B}^2$ for a 2-manifold of genus-zero or with a single boundary, and applied in various tasks of computer vision including surface remeshing, registration, texture mapping, morphing and retargeting [44]. The classical Poincaré-Klein-Koebe uniformization theorem shows that any genus-zero, genus-one and higher genus closed 2D surfaces are uniquely conformal to the surface with constant Gaussian curvatures 1, 0 and -1, respectively, and the associated universal covering spaces with the uniformization metrics can be isometrically embedded onto $\mathbb{S}^2$, $\mathbb{R}^2$ and $\mathbb{H}^2$ (hyperbolic space) with Euler characteristic numbers $\chi > 0$, $\chi = 0$ and $\chi < 0$, respectively. This indicates that the topological property of genus-one closed surfaces is different from others. More precisely, any genus-one closed surface can be periodically and conformally mapped to a parallelogram forming a tiling of the whole plane $\mathbb{C}$ with Euclidean metric. The parallelogram with equivalent left and right sides, as well as, upper and lower sides, respectively, isometrically forms a standard torus $\mathbb{T}^2$. For conformal parameterizations of genus-one or higher genus surfaces, some well-developed algorithms, such as the holomorphic 1-form [22, 23, 27] and the discrete Ricci flow [26, 48] have been proposed.

Because of the special topological property of genus-one closed surfaces, in this paper, we are motivated to study the area- and volume-preserving parameterizations of genus-one 2- and

3-manifolds, respectively. For the further applications of the genus-one 3-manifold (toroidal polyhedron), we mainly focus on developing an efficient algorithm for the computation of the volume-preserving parameterizations between genus-one 3-manifolds and the standard solid torus $\mathbb{T}^3$. The basic approach is first to conformally map the boundary of the genus-one 3-manifold onto a standard $\mathbb{T}^2$ by computing the holomorphic 1-forms [22]. Then the boundary map is equiareally deformed to an area-preserving map on $\mathbb{T}^2$ by minimizing the stretch energy. Finally, the volume-preserving parameterization between the genus-one 3-manifold and the solid torus $\mathbb{T}^3$ is computed by minimizing the volumetric stretch energy. The contribution of this paper can be divided into the following three parts.

(i) Universality: The newly developed stretch energy minimization can be utilized to find the area-preserving (equiareal) parameterizations between genus-one closed surfaces and $\mathbb{T}^2$, as well as the volume-preserving parameterizations between genus-one 3-manifolds and the solid torus $\mathbb{T}^3$.

(ii) Effectiveness and reliability: The proposed area-preserving parameterization algorithm for genus-one closed surfaces converges well within 5 iterations, the average of ratios between local areas of triangular faces is close to one up to $\pm 6 \times 10^{-4}$ and the resulting mappings for the benchmark mesh models are bijective. Furthermore, the proposed volume-preserving parameterization algorithm for genus-one 3-manifolds converges well within 20 iterations, the average of ratios between local volumes of tetrahedrons is close to one up to ± 0.03 and the percentage of bijectivity of tetrahedrons is higher than 99.9% by using the regularization technique.

(iii) Applications: Applications on the vertebra registrations and the volume-based manifold partitions can robustly be carried out by the proposed parameterization algorithm.

1.1. Notations and overview. The following notations are used in this paper. Other notations will be clearly defined whenever they appear.

- Bold letters, e.g. $\mathbf{u}$, $\mathbf{v}$, $\mathbf{w}$, denote (complex) vectors.
- Capital letters, e.g. A, B, C, denote matrices.
- Typewriter letters, e.g. $\mathtt{I}$, $\mathtt{J}$, $\mathtt{K}$, denote ordered sets of indices.
- $\mathbf{v}_i$ denotes the ith entry of the vector $\mathbf{v}$.
- $\mathbf{v}_\mathtt{I}$ denotes the subvector of $\mathbf{v}$ composed of $\mathbf{v}_i$, for $i \in \mathtt{I}$.
- $|\mathbf{v}|$ denotes the vector with the ith entry being $|\mathbf{v}_i|$.
- $\mathrm{diag}(\mathbf{v})$ denotes the diagonal matrix with the (i,i)th entry being $\mathbf{v}_i$.
- $A_{i,j}$ denotes the (i,j)th entry of the matrix A.
- $A_{\mathtt{I},\mathtt{J}}$ denotes the submatrix of A composed of $A_{i,j}$, for $i \in \mathtt{I}$ and $j \in \mathtt{J}$.
- $\mathbb{S}^n := \{\mathbf{x} \in \mathbb{R}^{n+1} \mid \|\mathbf{x}\| = 1\}$ denotes the n-sphere in $\mathbb{R}^{n+1}$.
- $\mathbb{B}^n := \{\mathbf{x} \in \mathbb{R}^{n} \mid \|\mathbf{x}\| \leq 1\}$ denotes the solid n-ball in $\mathbb{R}^n$.
- $[v_0, \ldots, v_m]$ denotes the m-simplex determined by the points $v_0, \ldots, v_m$.
- $|[v_0, \ldots, v_m]|$ denotes the volume of the m-simplex $[v_0, \ldots, v_m]$.
- i denotes the imaginary unit $\sqrt{-1}$.
- I_n denotes the identity matrix of size $n \times n$.
- $\mathbf{0}$ denotes the zero vectors and matrices of appropriate sizes.

This paper is organized as follows. First, we introduce the discrete manifolds and mappings as well as the computation of the conformal parameterization via the holomorphic differentials in Sections 2 and 3, respectively. Then, we propose a modified stretch and volumetric stretch energy minimization for the computation of the area- and volume-preserving parameterizations in Sections 4 and 5, respectively. Numerical experiments of the proposed algorithms are presented in Section 6. Applications on Vertebra registrations and partitions are demonstrated in Section 7. Concluding remarks are given in Section 8.

2. Discrete 3-manifolds and parameterizations. In this paper, we consider discrete 3-manifolds embedded in $\mathbb{R}^3$ with a single boundary being a genus-one closed 2D surface. In real applications, a discrete 3-manifold can be represented as a tetrahedral mesh $\mathcal{M}$, which is consisted of n vertices with coordinates in $\mathbb{R}^3$

$$\mathcal{V}(\mathcal{M}) = \left\{ v_s \equiv \left(v_s^1, v_s^2, v_s^3\right)^\top \in \mathbb{R}^3 \right\}_{s=1}^{n}$$

and tetrahedrons

$$\mathcal{T}(\mathcal{M}) = \left\{ [v_i, v_j, v_k, v_\ell] \subset \mathbb{R}^3 \text{ for some vertices } \{v_i, v_j, v_k, v_\ell\} \subset \mathcal{V}(\mathcal{M}) \right\},$$

where the bracket $[v_i, v_j, v_k, v_\ell]$ denotes the *convex hull* (3-simplex) of the affinely independent points $\{v_i, v_j, v_k, v_\ell\}$. Furthermore, the sets of triangular faces and edges of the mesh $\mathcal{M}$ are denoted by

$$\mathcal{F}(\mathcal{M}) = \{[v_i, v_j, v_k] \mid [v_i, v_j, v_k, v_\ell] \in \mathcal{T}(\mathcal{M}) \text{ for some } v_\ell \in \mathcal{V}(\mathcal{M})\}$$

and

$$\mathcal{E}(\mathcal{M}) = \{[v_i, v_j] \mid [v_i, v_j, v_k] \in \mathcal{F}(\mathcal{M}) \text{ for some } v_k \in \mathcal{V}(\mathcal{M})\},$$

respectively. The union of $\mathcal{V}(\mathcal{M})$, $\mathcal{E}(\mathcal{M})$, $\mathcal{F}(\mathcal{M})$ and $\mathcal{T}(\mathcal{M})$ forms a homogeneous simplicial 3-complex. Similarly, a 2-manifold is called a *surface*, which is represented as a triangular mesh consisted of vertices and triangular faces.

A piecewise affine mapping $f : \mathcal{M} \to \mathbb{R}^3$ is defined as a matrix

$$\mathbb{f} = \begin{bmatrix} f(v_1) & \cdots & f(v_n) \end{bmatrix}^\top \equiv \begin{bmatrix} \mathbb{f}_1 & \cdots & \mathbb{f}_n \end{bmatrix}^\top \in \mathbb{R}^{n\times 3}. \tag{2.1}$$

For a point $v \in \mathcal{M}$ belonging to some tetrahedron $[v_i, v_j, v_k, v_\ell] \in \mathcal{T}(\mathcal{M})$, the value $f(v)$ is defined as a linear combination of $\mathbb{f}_i$, $\mathbb{f}_j$, $\mathbb{f}_k$ and $\mathbb{f}_\ell$

$$f|_{[v_i,v_j,v_k,v_\ell]}(v) = \lambda_i(v)\,\mathbb{f}_i + \lambda_j(v)\,\mathbb{f}_j + \lambda_k(v)\,\mathbb{f}_k + \lambda_\ell(v)\,\mathbb{f}_\ell$$

with coefficients $\lambda_i(v) = \frac{|[v,v_j,v_k,v_\ell]|}{|[v_i,v_j,v_k,v_\ell]|}$, $\lambda_j(v) = \frac{|[v_i,v,v_k,v_\ell]|}{|[v_i,v_j,v_k,v_\ell]|}$, $\lambda_k(v) = \frac{|[v_i,v_j,v,v_\ell]|}{|[v_i,v_j,v_k,v_\ell]|}$ and $\lambda_\ell(v) = \frac{|[v_i,v_j,v_k,v]|}{|[v_i,v_j,v_k,v_\ell]|}$ being the *barycentric coordinates* of v in $[v_i, v_j, v_k, v_\ell]$. Here the absolute value $|[v_0, \ldots, v_m]|$ denotes the volume of the m-simplex $[v_0, \ldots, v_m]$. In particular, $|[v_i, v_j, v_k, v_\ell]|$, $|[v_i, v_j, v_k]|$ and $|[v_i, v_j]|$ denote the volume, area and length of the tetrahedron $[v_i, v_j, v_k, v_\ell]$, triangle $[v_i, v_j, v_k]$ and interval $[v_i, v_j]$, respectively.

In this paper, we consider developing an algorithm for the computation of a bijective volume-preserving parameterization between a genus-one 3-manifold $\mathcal{M} \subset \mathbb{R}^3$ and the standard solid torus $\mathbb{T}^3$. A parameterization $f : \mathcal{M} \to \mathbb{T}^3$ is said to be volume-preserving if the Jacobian matrix $J_{f^{-1}} = [\frac{\partial f^{-1}}{\partial u^1}, \frac{\partial f^{-1}}{\partial u^2}, \frac{\partial f^{-1}}{\partial u^3}]$ satisfies

$$\det\left(J_{f^{-1}}(u^1, u^2, u^3)\right) = 1.$$

Table 3.1

The length of loops γ_1, γ_2, and the execution time cost (sec.) of the homology group basis by the minimal spanning tree method provided in Chapter 9 of [24] and the Reeb graph method [14]. $\#\mathcal{F}(\partial\mathcal{M})$ denotes the number of triangular faces of the model.

Model Name	$\#\mathcal{F}(\partial\mathcal{M})$	Minimal Spanning Tree			Reeb Graph		
		$\lvert\gamma_1\rvert$	$\lvert\gamma_2\rvert$	Time	$\lvert\gamma_1\rvert$	$\lvert\gamma_2\rvert$	Time
Petal	14,506	1.6486	6.4235	0.58	1.1012	4.3046	0.51
Vertebra	16,420	7.0326	2.0194	0.66	1.0358	1.9880	0.59
Rocker Arm	25,182	2.8960	2.7636	0.95	2.0576	2.3290	0.87
Kitten	21,584	3.4239	1.3030	0.89	0.4661	1.5106	0.73

In other words, f preserves the local volume. Additionally, a parameterization $f : \partial\mathcal{M} \to \mathbb{T}^2$ is said to be area-preserving or angle-preserving (conformal) if the first fundamental form $\mathrm{I}_{f^{-1}}$ satisfies $\det\left(\mathrm{I}_{f^{-1}}(u^1, u^2)\right) = 1$, i.e., f preserves the local area, or $\mathrm{I}_{f^{-1}}(u^1, u^2) = \lambda(u^1, u^2)I_2$, for some positive scaling function λ, i.e., f preserves local angles.

3. Conformal parameterizations via holomorphic differentials. Given a genus-g closed surface $\partial\mathcal{M}$. Based on the Hodge Theorem for the isomorphism between the de Rham cohomology group and the harmonic 1-form group, Gu and Yau [22, 23] [24, Chap. 11] developed an elegant numerical algorithm via holomorphic differentials for the computation of holomorphic 1-forms, and further the conformal map between $\partial\mathcal{M}$ and the g connected sum of $\mathbb{T}^2$, namely, $\mathbb{T}^2\#\cdots\#\mathbb{T}^2 = (\mathbb{T}^2\backslash\mathbb{D}^2)\cup\cdots\cup(\mathbb{T}^2\backslash\mathbb{D}^2)$. The procedure consists of four steps: (i) computing a basis for the cohomology group, (ii) computing a basis for the harmonic 1-form group, (iii) computing the corresponding holomorphic 1-forms, and (iv) integrating the holomorphic 1-forms to the holomorphic maps.

3.1. Homology and cohomology groups. The handle and tunnel loops $\{\gamma_1, \ldots, \gamma_{2g}\}$ on the genus-g closed surface $\partial\mathcal{M}$ form a basis for the homology group $H_1(\partial\mathcal{M})$. The basis can be efficiently computed by, e.g., the minimal spanning tree method [24, Chap. 9, Alg. 6] and the Reeb graph method [14].

In this subsection, we first compare these two algorithms in terms of efficiency and lengths of resulting loops for the computation of a basis for the homology group of a genus-one closed surface. The minimal spanning tree method and the Reeb graph method are performed by the software `RiemannMapper` and `ReebHanTun` developed by Gu [7] and Dey et al. [3], respectively. In Table 3.1, we see that the execution time of these two methods is similar, however, the resulting loops by the Reeb graph method have significantly shorter lengths compared to the loops by the minimal spanning tree method. Therefore, in this paper, we adopt the Reeb graph method in [14] for the computation of a basis for the homology group.

A 1-form $\eta : \mathcal{E}(\partial\mathcal{M}) \to \mathbb{R}$ is said to be closed if for each face $[v_i, v_j, v_k] \in \mathcal{F}(\partial\mathcal{M})$, it holds

$$\eta([v_i, v_j]) + \eta([v_j, v_k]) + \eta([v_k, v_i]) = 0.$$

Each handle or tunnel loop γ_ℓ corresponds to a characteristic closed 1-form $\eta_\ell : \mathcal{E}(\partial\mathcal{M}) \to \mathbb{R}$ defined as

$$\eta_\ell([v_i, v_j]) = f_\ell(v_j) - f_\ell(v_i) \tag{3.1a}$$

with

$$f_\ell(v) = \begin{cases} 1 & \text{if } v \in \gamma_\ell^+, \\ 0 & \text{otherwise}, \end{cases} \tag{3.1b}$$

where $\gamma_\ell^+ \cup \gamma_\ell^-$ forms the boundary of the open mesh $\partial\mathcal{M}_\ell$ by slicing $\partial\mathcal{M}$ along γ_ℓ, for $\ell = 1, \ldots, 2g$. The set of characteristic closed 1-forms $\{\eta_1, \ldots, \eta_{2g}\}$ form a basis for the cohomology group $H^1(\partial\mathcal{M})$.

3.2. Harmonic 1-form ([24, Section 11.5]). For each vertex $v_i \in \mathcal{V}(\partial\mathcal{M})$, let $N(v_i) = \{v_j \,|\, [v_i, v_j] \in \mathcal{E}(\partial\mathcal{M})\}$ denote the one-ring neighborhood of v_i. The weighted coefficient $w_{i,j}$ of the discrete Laplacian operator $\triangle_{\partial\mathcal{M}}$ is given by the cotangent weight

$$w_{i,j} = \frac{\cot\theta_{i,j} + \cot\theta_{j,i}}{2}, \tag{3.2}$$

where $\theta_{i,j}$ and $\theta_{j,i}$ are two angles opposite to the edge $[v_i, v_j]$ connecting vertices v_i and v_j on the mesh $\partial\mathcal{M}$.

A closed 1-form ω is said to be a harmonic 1-form, if it is locally gradient of some harmonic function $h : \mathcal{V}(\partial\mathcal{M}) \to \mathbb{R}$. In other words, a harmonic 1-form ω satisfies

$$\begin{aligned} (\triangle_{\partial\mathcal{M}} h)(v_i) &= \sum_{v_j \in N(v_i)} w_{i,j}\, \mathrm{d}h([v_i, v_j]) = \sum_{v_j \in N(v_i)} w_{i,j}\,(h(v_j) - h(v_i)) \\ &= \sum_{v_j \in N(v_i)} w_{i,j}\omega([v_i, v_j]) = 0. \end{aligned} \tag{3.3}$$

Given a closed 1-form η, from the Hodge theorem [24, Chap. 4], the unique harmonic 1-form ω cohomologous to η is given by

$$\omega([v_i, v_j]) = \eta([v_i, v_j]) + h(v_j) - h(v_i), \tag{3.4}$$

where the unknown function $h : \mathcal{V}(\partial\mathcal{M}) \to \mathbb{R}$ is solved from the linear system

$$\sum_{v_j \in N(v_i)} w_{i,j}\,(\eta([v_i, v_j]) + h(v_j) - h(v_i)) = 0, \quad \text{for each } v_i \in \mathcal{V}(\partial\mathcal{M}). \tag{3.5}$$

3.3. Conjugate 1-form ([24, Sec. 11.6]). Note that every closed 1-form ω corresponds to a vector-valued 2-form $\boldsymbol{\omega} : \mathcal{F}(\partial\mathcal{M}) \to \mathbb{R}^3$ satisfying

$$\begin{cases} \boldsymbol{\omega}([v_i, v_j, v_k])^\top (v_j - v_i) = \omega([v_i, v_j]), \\ \boldsymbol{\omega}([v_i, v_j, v_k])^\top (v_k - v_j) = \omega([v_j, v_k]), \\ \boldsymbol{\omega}([v_i, v_j, v_k])^\top (v_i - v_k) = \omega([v_k, v_i]). \end{cases}$$

The 2-form $\boldsymbol{\omega}$ can be explicitly formulated as

$$\boldsymbol{\omega}([v_i, v_j, v_k]) = \frac{(\omega([v_i, v_j])v_k + \omega([v_k, v_i])v_j + \omega([v_j, v_k])v_i) \times \mathbf{n}([v_i, v_j, v_k])}{2|[v_i, v_j, v_k]|}. \tag{3.6}$$

On the other hand, the Hodge conjugate of $\boldsymbol{\omega}$, a vector-valued 2-form $\star\boldsymbol{\omega} : \mathcal{F}(\partial\mathcal{M}) \to \mathbb{R}^3$, is defined as

$$\star\,\boldsymbol{\omega}(\tau) = \mathbf{n}(\tau) \times \boldsymbol{\omega}(\tau), \tag{3.7}$$

where $\mathbf{n}(\tau)$ is the normal vector of the triangular face τ.

Under a basis of harmonic 1-forms $\{\omega_1, \ldots, \omega_{2g}\}$, each harmonic 1-form ω can be written as the linear combination of $\{\omega_m\}_{m=1}^{2g}$. Suppose the Hodge conjugate $\star\omega$ of the harmonic 1-form ω is represented as

$$\star\,\omega = \sum_{m=1}^{2g} \mu_m \omega_m. \tag{3.8}$$

Then, the unknown coefficients $\{\mu_m\}_{m=1}^{2g}$ must satisfy

$$\int_{\partial\mathcal{M}} \omega_\ell \wedge \star\omega = \sum_{m=1}^{2g} \mu_m \int_{\partial\mathcal{M}} \omega_\ell \wedge \omega_m, \tag{3.9}$$

for $\ell = 1, \ldots, 2g$. Note that the 2-forms $\omega_\ell \wedge \star\omega$ and $\omega_\ell \wedge \omega_m$ from $\mathcal{F}(\partial\mathcal{M})$ to $\mathbb{R}$ can be computed by

$$(\omega_\ell \wedge \star\omega)(\tau) = \boldsymbol{\omega}_\ell(\tau) \times \star\boldsymbol{\omega}(\tau) \cdot \mathbf{n}(\tau)|\tau|,$$

and

$$(\omega_\ell \wedge \omega_m)(\tau) = \boldsymbol{\omega}_\ell(\tau) \times \boldsymbol{\omega}_m(\tau) \cdot \mathbf{n}(\tau)|\tau|,$$

for each $\tau \in \mathcal{F}(\partial\mathcal{M})$. It follows that

$$b_\ell \equiv \int_{\partial\mathcal{M}} \omega_\ell \wedge \star\omega = \sum_{\tau\in\mathcal{F}(\partial\mathcal{M})} \boldsymbol{\omega}_\ell(\tau) \times \star\boldsymbol{\omega}(\tau) \cdot \mathbf{n}(\tau)|\tau|, \tag{3.10}$$

and

$$c_{\ell,m} \equiv \int_{\partial\mathcal{M}} \omega_\ell \wedge \omega_m = \sum_{\tau\in\mathcal{F}(\partial\mathcal{M})} \boldsymbol{\omega}_\ell(\tau) \times \boldsymbol{\omega}_m(\tau) \cdot \mathbf{n}(\tau)|\tau|,$$

for $\ell, m = 1, \ldots, 2g$. As a result, the coefficients $\{\mu_m\}_{m=1}^{2g}$ can be obtained by solving the linear system

$$\begin{bmatrix} 0 & c_{1,2} & \cdots & c_{1,2g} \\ -c_{1,2} & 0 & \cdots & c_{2,2g} \\ \vdots & \vdots & \ddots & \vdots \\ -c_{1,2g} & -c_{2,2g} & \cdots & 0 \end{bmatrix} \begin{bmatrix} \mu_1 \\ \mu_2 \\ \vdots \\ \mu_{2g} \end{bmatrix} = \begin{bmatrix} b_1 \\ b_2 \\ \vdots \\ b_{2g} \end{bmatrix}. \tag{3.11}$$

Ultimately, a basis for holomorphic 1-forms is given by

$$\{\zeta_\ell = \omega_\ell + \mathrm{i}\star\omega_\ell\}_{\ell=1}^{2g}. \tag{3.12}$$

Note that each holomorphic 1-form ζ on $\partial\mathcal{M}$ can be represented as the linear combination $\zeta = \sum_{\ell=1}^{2g} \alpha_\ell \zeta_\ell$ with $\alpha_\ell \in \mathbb{R}$.

3.4. Visualization of the fundamental domain. In particular, to compute the conformal map of a genus-one closed surface $\partial\mathcal{M}$ induced by the holomorphic 1-form ζ, we first slice $\partial\mathcal{M}$, respectively, along the handle and the tunnel loops in a basis of $H_1(\partial\mathcal{M})$. The only intersecting vertex of these two loops on the mesh $\partial\mathcal{M}$ is separated into 4 corner vertices $v_{\mathtt{C}(1)}, \ldots, v_{\mathtt{C}(4)}$ counterclockwise on the sliced mesh $\partial\widetilde{\mathcal{M}}$. Choosing the vertex $v_0 \equiv v_{\mathtt{C}(1)} \in \partial\widetilde{\mathcal{M}}$ as the origin, for each $v_t \in \mathcal{V}(\partial\widetilde{\mathcal{M}})$, we integrate ζ along a curve $\gamma(v_0, v_t)$ from v_0 to v_t (see [24, Alg. 35] for details) as

$$z_t := x_t + \mathrm{i}y_t = \int_{\gamma(v_0,v_t)} \zeta. \tag{3.13}$$

The image of the mapping $f_{\mathbb{C}} : \partial\widetilde{\mathcal{M}} \to \mathbb{C}$ given by $f_{\mathbb{C}}(v_t) = z_t$ is known as the fundamental domain of the genus-one surface $\partial\mathcal{M}$.

Note that the polygon formed by $z_{\mathtt{C}(1)}, \ldots, z_{\mathtt{C}(4)}$, in general, is a parallelogram. In order to obtain a fundamental domain with four corner vertices forming a rectangle, we first compute

$$a_{1,1} = \int_{\gamma(v_{\mathtt{C}(1)}, v_{\mathtt{C}(2)})} \zeta_1, \quad a_{1,2} = \int_{\gamma(v_{\mathtt{C}(1)}, v_{\mathtt{C}(4)})} \zeta_1, \quad a_{2,1} = \int_{\gamma(v_{\mathtt{C}(1)}, v_{\mathtt{C}(2)})} \zeta_2, \quad a_{2,2} = \int_{\gamma(v_{\mathtt{C}(1)}, v_{\mathtt{C}(4)})} \zeta_2,$$

where $\{\zeta_1, \zeta_2\}$ is given in (3.12). We find an optimal coefficient $\beta \in [0,1]$ so that $(1-\beta)a_{1,1} + \beta a_{2,1}$ is as perpendicular as possible to $(1-\beta)a_{1,2} + \beta a_{2,2}$. That is, β satisfies

$$\beta = \operatorname*{argmin}_{\beta\in[-1,1]} \mathrm{Re}\left(((1-\beta)a_{1,1} + \beta a_{2,1})\overline{((1-\beta)a_{1,2} + \beta a_{2,2})}\right)^2. \tag{3.14}$$

The desired holomorphic 1-form ζ in (3.13) is then given by $\zeta = (1-\beta)\zeta_1 + \beta\zeta_2$.

Finally, the rectangle fundamental domain $f_{\mathbb{C}}(\partial\widetilde{\mathcal{M}})$ is conformally mapped to $\mathbb{T}^2$ by $f_{\mathbb{T}^2} : \mathbb{C} \to \mathbb{T}^2$ defined as

$$f_{\mathbb{T}^2}(x_t + \mathrm{i}y_t) = \left(\frac{r \sin \frac{2\pi x_t}{\max_t(x_t)}}{\sqrt{r^2+1} - \cos\frac{2\pi y_t}{\max_t(y_t)}}, \frac{r \cos \frac{2\pi x_t}{\max_t(x_t)}}{\sqrt{r^2+1} - \cos\frac{2\pi y_t}{\max_t(y_t)}}, \frac{\sin \frac{2\pi y_t}{\max_t(y_t)}}{\sqrt{r^2+1} - \cos\frac{2\pi y_t}{\max_t(y_t)}} \right), \tag{3.15}$$

where $r = \sqrt{(\frac{a}{b})^2 - 1}$ in which a and b are the side lengths of the rectangle $f_{\mathbb{C}}(\partial\widetilde{\mathcal{M}})$ with $a > b$. Note that the radius of the tube is $\frac{1}{r}$ and the distance from the center of the tube to the center of the torus is $\sqrt{1+r^2}/r$. The conformal mapping (3.15) is adopted from a formula in [39] by changing the periods of x-direction and y-direction to be $\max_t(x_t)$ and $\max_t(y_t)$, respectively.

The computational procedure for Subsections 3.1 to 3.4 is summarized in Algorithm 3.1.

4. Area-preserving parameterizations. In this section, we propose a modified stretch energy minimization (SEM) for the computation of the area-preserving parameterization between a genus-one closed triangular mesh $\partial\mathcal{M}$ and $\mathbb{T}^2$. Let $g : \partial\mathcal{M} \to \mathbb{T}^2$ be a piecewise affine mapping satisfying

$$\mathrm{g} = [g(v_1), \cdots, g(v_n)]^\top = [\mathrm{g}_1, \cdots, \mathrm{g}_n]^\top \in \mathbb{R}^{n\times 3} \text{ with } \mathrm{g}_i \in \mathbb{T}^2,$$

Algorithm 3.1 Conformal Parameterization on $\mathbb{T}^2$

Input: A genus-one closed triangular mesh $\partial\mathcal{M}$.

Output: A conformal mapping g that maps $\partial\mathcal{M}$ to a standard torus $\mathbb{T}^2$.

1: Compute a basis $\{\gamma_1, \gamma_2\}$ for the homology group $H_1(\partial\mathcal{M})$ by `ReebHanTun` [3].
2: Compute the dual basis (characteristic closed 1-form) $\{\eta_1, \eta_2\}$ for $H^1(\partial\mathcal{M})$ by (3.1).
3: Compute the harmonic 1-form basis $\{\omega_1, \omega_2\}$ for $H^1(\partial\mathcal{M})$ by (3.2)–(3.5).
4: Compute the holomorphic 1-form basis $\{\zeta_\ell = \omega_\ell + \mathrm{i} \star \omega_\ell\}_{\ell=1}^2$ by (3.6)–(3.11).
5: Compute the holomorphic 1-form $\zeta = (1-\beta)\zeta_1 + \beta\zeta_2$, where β is given by (3.14).
6: Slice $\partial\mathcal{M}$ along γ_1 and γ_2 into $\partial\widetilde{\mathcal{M}}$.
7: Compute the holomorphic mapping $f_{\mathbb{C}} : \partial\widetilde{\mathcal{M}} \to \mathbb{C}$ by (3.13).
8: Map the rectangle to the standard torus by $f_{\mathbb{T}^2} : \mathbb{C} \to \mathbb{T}^2$ as in (3.15).
9: **return** $g \equiv f_{\mathbb{T}^2} \circ f_{\mathbb{C}}|_{\partial\mathcal{M}}$.

for $v_i \in \mathcal{V}(\partial\mathcal{M})$, $i = 1, \ldots, n$. Based on the original SEM algorithm [47] aiming to compute the disk-shaped equiareal parameterizations of simply connected open surfaces, we try finding an area-preserving mapping $g : \partial\mathcal{M} \to \mathbb{T}^2$ by minimizing the modified stretch energy functional

$$\mathcal{E}_S(g) = \frac{1}{2}\mathrm{trace}\left(\mathrm{g}^\top L_S(g)\, \mathrm{g}\right) - |g(\partial\mathcal{M})|, \tag{4.1}$$

where $|g(\partial\mathcal{M})|$ denotes the area of the image $g(\partial\mathcal{M})$, $L_S(g)$ is the stretch Laplacian matrix with

$$[L_S(g)]_{i,j} = \begin{cases} w_{i,j}(g) \equiv -\frac{1}{2}\left(\frac{\cot(\theta_{i,j}(g))}{\sigma_{g^{-1}}([v_i,v_j,v_k])} + \frac{\cot(\theta_{j,i}(g))}{\sigma_{g^{-1}}([v_j,v_i,v_\ell])}\right) & \text{if } [v_i, v_j] \in \mathcal{E}(\partial\mathcal{M}), \\ -\sum_{\ell \neq i} w_{i,\ell}(g) & \text{if } j = i, \\ 0 & \text{otherwise} \end{cases} \tag{4.2}$$

in which $\theta_{i,j}(g)$ and $\theta_{j,i}(g)$ are two angles opposite to the edge $[g(v_i), g(v_j)]$ connecting vertices $g(v_i)$ and $g(v_j)$ on $\mathbb{T}^2$, as illustrated in Fig. 4.1, and

$$\sigma_{g^{-1}}(\tau) = \frac{|\tau|}{|g(\tau)|} \tag{4.3}$$

is the stretch factor of g on the triangular face $\tau \in \mathcal{F}(\partial\mathcal{M})$. The modified SEM algorithm for genus-one closed triangular meshes $\partial\mathcal{M}$ is stated as follows. We first compute the conformal mapping $g^{(0)} : \partial\mathcal{M} \to \mathbb{T}^2$ by Algorithm 3.1 as an initial map. Then, for $k = 1, 2, \ldots$, and $\ell = 1, 2$, we imitate the steps of (3.3)–(3.5) and (3.12)–(3.15) by modifying the stretch Laplacian matrix $L_S(g^{(k-1)})$ as in (4.2) at each k-iteration and compute the stretched harmonic 1-form $\omega_\ell^{(k)} : \mathcal{E}(\partial\mathcal{M}) \to \mathbb{R}$ by

$$\omega_\ell^{(k)}([v_i, v_j]) = \eta_\ell([v_i, v_j]) + h_\ell^{(k)}(v_j) - h_\ell^{(k)}(v_i) \tag{4.4}$$

in which η_ℓ is the characteristic closed 1-form defined in (3.1), and the unknown function $h_\ell^{(k)} : \mathcal{V}(\partial\mathcal{M}) \to \mathbb{R}$ is solved from the linear system

$$\sum_{v_j \in N(v_i)} \left[L_S(g^{(k-1)})\right]_{i,j} \left(\eta_\ell([v_i, v_j]) + h_\ell^{(k)}(v_j) - h_\ell^{(k)}(v_i)\right) = 0, \tag{4.5}$$

for each $v_i \in \mathcal{V}(\partial\mathcal{M})$. The Hodge conjugate $\star\omega_\ell^{(k)}$ of the stretched harmonic 1-form $\omega_\ell^{(k)}$ is computed as in Subsection 3.3. The stretched harmonic 1-form is then given by

$$\zeta_\ell^{(k)} = \omega_\ell^{(k)} + \mathrm{i}\star\omega_\ell^{(k)}, \;\; \ell = 1,2. \tag{4.6}$$

By integrating $\zeta_\ell^{(k)}$ as in (3.13), we obtain the mapping $(f_\mathbb{C})_\ell^{(k)} : \partial\widetilde{\mathcal{M}} \to \mathbb{C}$, for $\ell = 1,2$. Similar to Subsection 3.4, we find an optimal coefficient $\beta \in [0,1]$ by (3.14) so that the parallelogram form by corners of the mapping

$$f_\mathbb{C}^{(k)} = (1-\beta)(f_\mathbb{C})_1^{(k)} + \beta(f_\mathbb{C})_2^{(k)} \tag{4.7}$$

is as close to a rectangle as possible.

Note that the corner vertices are mapped into the four corners $(0,0)$, $\mathbf{p}^{(k)} = (p_1^{(k)}, p_2^{(k)})$, $\mathbf{q}^{(k)} = (q_1^{(k)}, q_2^{(k)})$, $\mathbf{r}^{(k)} = (r_1^{(k)}, r_2^{(k)})$ of a parallelogram with width $a^{(k)}$ and height $b^{(k)}$. In order to map the fundamental domain to a standard torus $\mathbb{T}^2$, we first map the parallelogram to a rectangle of the side lengths $a^{(k)}$ and $b^{(k)}$ with $a^{(k)} > b^{(k)}$, by an affine mapping $\varphi^{(k)} : \mathbb{C} \to \mathbb{R}^2$ given by

$$\varphi^{(k)}(x + \mathrm{i}y) = P^{(k)} \begin{bmatrix} x \\ y \end{bmatrix} + \mathbf{t}^{(k)}, \tag{4.8a}$$

where $P^{(k)} \in \mathbb{R}^{2\times 2}$ is a matrix with $\det P^{(k)} \neq 0$ and $\mathbf{t}^{(k)} \in \mathbb{R}^2$ is a translation vector. The matrix $P^{(k)}$ and the vector $\mathbf{t}^{(k)}$ can be determined by the equation

$$\begin{bmatrix} P^{(k)} & \mathbf{t}^{(k)} \\ \mathbf{0}^\top & 1 \end{bmatrix} = \begin{bmatrix} p_1^{(k)} & q_1^{(k)} & r_1^{(k)} \\ p_2^{(k)} & q_2^{(k)} & r_2^{(k)} \\ 1 & 1 & 1 \end{bmatrix} \begin{bmatrix} 0 & a^{(k)} & a^{(k)} \\ b^{(k)} & b^{(k)} & 0 \\ 1 & 1 & 1 \end{bmatrix}^{-1}. \tag{4.8b}$$

Alternatively, the affine mapping $\varphi^{(k)}$ can be directly computed using the MATLAB built-in function `fitgeotrans`. Note that the affine mapping $\varphi^{(k)}$ is area-preserving, but not angle-preserving which cannot be used in Subsection 3.4.

The updated torus mapping $g^{(k)} : \partial\mathcal{M} \to \mathbb{T}^2$ is given by

$$g^{(k)} := f_{\mathbb{T}^2} \circ \varphi^{(k)} \circ f_\mathbb{C}^{(k)},$$

where $f_{\mathbb{T}^2}$ is the map from the rectangle fundamental domain to $\mathbb{T}^2$ as in (3.15). The sequence $\{g^{(k)}\}_{k\in\mathbb{N}}$ would numerically converge to an area-preserving mapping $g^{(*)} : \partial\mathcal{M} \to \mathbb{T}^2$.

The computational procedure for the area-preserving parameterization is summarized in Algorithm 4.1.

Remark. *(i) Imitating Algorithm 3.1, we have the following iteration:*

$$g^{(k-1)} \xrightarrow{(4.2)} L_S(g^{(k-1)}) \xrightarrow[(4.6)]{(4.4)} \zeta_\ell^{(k)} \xrightarrow[(4.7)]{(3.13)} f_\mathbb{C}^{(k)} \xrightarrow[(3.15)]{(4.8)} f_{\mathbb{T}^2} \circ \varphi^{(k)} \circ f_\mathbb{C}^{(k)} := g^{(k)}.$$

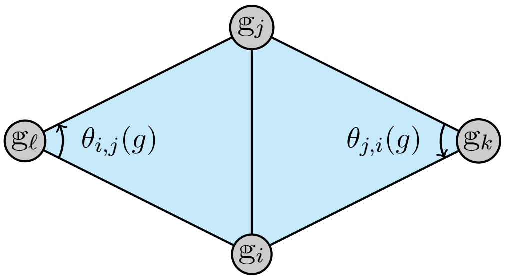

Figure 4.1. *An illustration for the cotangent weights.*

Algorithm 4.1 Modified SEM for Area-Preserving Parameterization on $\mathbb{T}^2$

Input: A genus-one closed triangular mesh $\partial\mathcal{M}$.
Output: An area-preserving mapping g that maps $\partial\mathcal{M}$ to a standard torus $\mathbb{T}^2$.

Compute a conformal mapping $g : \partial\mathcal{M} \to \mathbb{T}^2$ by Algorithm 3.1.
while not convergent **do**
  Update $L \leftarrow L_S(g)$ as in (4.2).
  Update the 1-forms $\{\omega_1, \omega_2\}$ as in (4.4) and (4.5).
  Compute the 1-forms $\{\zeta_\ell = \omega_\ell + \mathrm{i} \star \omega_\ell\}_{\ell=1}^2$.
  Compute mappings $\{(f_\mathbb{C})_\ell\}_{\ell=1}^2$ by integrating $\{\zeta_\ell\}_{\ell=1}^2$, respectively, as (3.13).
  Compute the parallelogram mapping $f_\mathbb{C} : \partial\widetilde{\mathcal{M}} \to \mathbb{C}$ as in (4.7).
  Map the parallelogram into a rectangle of width a and height b by the affine transformation φ as in (4.8).
  Map the rectangle to the standard torus by $f_{\mathbb{T}^2} : \mathbb{C} \to \mathbb{T}^2$ defined as (3.15).
  Update $g \leftarrow f_{\mathbb{T}^2} \circ \varphi \circ f_\mathbb{C}|_{\partial\mathcal{M}}$.
end while
return g.

In fact, we solve the energy minimization problem of (4.1) with the constraint $g : \partial\mathcal{M} \to \mathbb{T}^2$ via sequential quadratic optimizations by regarding $L_S(g^{(k-1)})$ as a matrix independent of $g^{(k)}$. At each kth iteration, we solve the quadratic optimization problem

$$\mathcal{E}_S^{(k)}(g) = \frac{1}{2}\mathrm{trace}\left(\mathrm{g}^\top L_S(g^{(k-1)})\,\mathrm{g}\right) - |g(\partial\mathcal{M})|$$

with $g : \partial\mathcal{M} \to \mathbb{T}^2$ as follows. We first consider solving the critical point of the gradient equation for $f : \partial\widetilde{\mathcal{M}} \to \mathbb{C}$

$$\nabla\mathcal{E}_S^{(k)}(f) = L_S(g^{(k-1)})\,\mathrm{f} = \mathbf{0}.$$

From the fact that $\sum_{v_j \in N(v_i)} \left[L_S(g^{(k-1)})\right]_{i,j} \zeta_\ell^{(k)}([v_i, v_j]) = 0$ by (4.4)–(4.6) follows that

$$L_S(g^{(k-1)})\,\mathrm{f}_\mathbb{C}^{(k)} = 0,$$

where $\mathrm{f}_\mathbb{C}^{(k)}$ is the matrix representation of $f_\mathbb{C}^{(k)}$ at $\mathcal{V}(\partial\widetilde{\mathcal{M}})$. Then, to guarantee the image being a torus $\mathbb{T}^2$, we use the bijective maps (3.15) and (4.8) to project the fundamental domain of the image of $f_\mathbb{C}^{(k)}$ back to $\mathbb{T}^2$ by setting $g^{(k)} := f_{\mathbb{T}^2} \circ \varphi^{(k)} \circ f_\mathbb{C}^{(k)}$.

(ii) Since the constrained energy minimization problem of (4.1) with the imposed condition $\sigma_{g^{-1}} = |\tau|/|g(\tau)|$ in (4.3) is highly nonlinear, the convergence of the stretch factors of (4.3) and the stretch energy of (4.1) is hard to be proved theoretically. However, we can numerically check the convergence behavior of the stretch energy and the total area distortion, and the stretch factors in Figures 6.6 and 6.7, respectively. In Figure 6.6, we observe that Algorithm 4.1 drops very fast in the first 5 steps and then goes down very gently in the last 15 steps that is very similar to a sublinear convergence behavior. It can be expected that the convergence rate of Algorithm 4.1 is of $O(1/k^s)$ with $1 \leq s \leq 2$.

(iii) The main differences between the proposed modified SEM algorithm and the SEM in [44] are: (1) The modified SEM aims to find a map $g : \mathcal{S} \to \mathbb{T}^2$ for a genus-one closed surface $\mathcal{S}$ while the original SEM aims to find a map $g : \mathcal{D} \to \mathbb{D}$ for a simply connected open surface $\mathcal{D}$. (2) The iteration is performed on computing the 1-form associated with the fundamental domain of $\mathbb{T}^2$ and the map is obtained by integrating the 1-form while the original SEM is performed directly on the disk-shaped image of the map.

5. Volume-preserving parameterization. In this section, we propose a modified volumetric stretch energy minimization (VSEM) algorithm for the computation of a volume-preserving parameterization between an n-vertex tetrahedral mesh $\mathcal{M}$ with a genus-one closed surface as the boundary and the standard solid torus $\mathbb{T}^3$. Let $f : \mathcal{M} \to \mathbb{T}^3$ be the piecewise affine mapping satisfying

$$\mathbb{f} = \begin{bmatrix} f(v_1) & \cdots & f(v_n) \end{bmatrix}^\top = \begin{bmatrix} \mathbb{f}_1 & \cdots & \mathbb{f}_n \end{bmatrix}^\top \in \mathbb{R}^{n\times 3} \quad \text{with } \mathbb{f}_i \in \mathbb{T}^3.$$

The *volumetric stretch energy functional* [45] on $\mathcal{M}$ is defined as

$$\mathcal{E}_{\mathbb{S}}(f) = \frac{1}{2}\text{trace}\left(\mathbb{f}^\top L_{\mathbb{S}}(f)\, \mathbb{f}\right), \tag{5.1}$$

where $L_{\mathbb{S}}(f)$ is the stretch volumetric Laplacian matrix with

$$[L_{\mathbb{S}}(f)]_{i,j} = \begin{cases} w_{i,j}(f) & \text{if } [v_i, v_j] \in \mathcal{E}(\mathcal{M}), \\ -\sum_{\ell \neq i} w_{i,\ell}(f) & \text{if } j = i, \\ 0 & \text{otherwise} \end{cases} \tag{5.2}$$

in which $w_{i,j}(f)$ is the modified cotangent weight [45] given by

$$w_{i,j}(f) = -\frac{1}{9} \sum_{\substack{\tau \in \mathcal{T}(\mathcal{M}) \\ [v_i,v_j]\cup[v_k,v_\ell]\subset\tau \\ [v_i,v_j]\cap[v_k,v_\ell]=\varnothing}} \frac{|f([v_i, v_k, v_\ell])||f([v_j, v_\ell, v_k])| \cos\theta_{i,j}^{k,\ell}(f)}{\boldsymbol{\sigma}_{f^{-1}}(\tau)\, |f(\tau)|}, \tag{5.3}$$

with $\boldsymbol{\sigma}_{f^{-1}}(\tau)$ being the stretch factor defined as

$$\boldsymbol{\sigma}_{f^{-1}}(\tau) = \frac{|\tau|}{|f(\tau)|}, \quad \text{for } \tau \in \mathcal{T}(\mathcal{M}). \tag{5.4}$$

Suppose an area-preserving parameterization $\mathbb{f}_{\mathtt{B}}^{(0)} \equiv g^{(*)}$ between $\partial\mathcal{M}$ and the torus $\mathbb{T}^2$ is computed by Algorithm 4.1. Then the volume-preserving parameterization between $\mathcal{M}$ and $\mathbb{T}^3$ is computed by minimizing the volumetric stretch energy (5.1) via the iteration

$$[L_{\mathbb{S}}(f^{(k)})]_{\mathtt{I},\mathtt{I}}\mathbb{f}_{\mathtt{I}}^{(k+1)} = -[L_{\mathbb{S}}(f^{(k)})]_{\mathtt{I},\mathtt{B}}\mathbb{f}_{\mathtt{B}}^{(0)}, \tag{5.5}$$

for solving the sequential quadratic programmings, where $\mathtt{B} = \{s \,|\, v_s \in \partial\mathcal{M}\}$, $\mathtt{I} = \{1,\ldots,n\}\backslash\mathtt{B}$ and the matrix $L_{\mathbb{S}}(f^{(k)})$ is updated by (5.2). The algorithm of the volumetric stretch energy minimization (VSEM) for the computation of the volume-preserving parameterizations between $\mathcal{M}$ and $\mathbb{T}^3$ is summarized in Algorithm 5.1.

Remark. *(i) As in Remark (i) of Section 4, Algorithm 5.1 solves the volumetric stretch energy minimization problem of (5.1) with the fixed area-preserving boundary constraint* $\mathbb{f}_{\mathtt{B}}^{(0)} : \partial\mathcal{M} \to \mathbb{T}^2$ *via sequential quadratic optimizations by regarding* $L_{\mathbb{S}}(f^{(k-1)})$ *as a matrix independent of* $f^{(k)}$. *At each kth step, the iteration (5.5) aims to find a critical* $\mathbb{f}^{(k)}$ *that satisfies*

$$\nabla\mathcal{E}_{\mathbb{S}}(f^{(k)}) = L_{\mathbb{S}}(f^{(k-1)})\mathbb{f}^{(k)} = \mathbf{0}.$$

Under the given torus-shaped boundary condition $\mathbb{f}_{\mathtt{B}}^{(0)}$, *the map* $f^{(k)}$ *can be computed by solving the linear system*

$$\begin{bmatrix} [L_{\mathbb{S}}(f^{(k-1)})]_{\mathtt{I},\mathtt{I}} & [L_{\mathbb{S}}(f^{(k-1)})]_{\mathtt{I},\mathtt{B}} \\ [L_{\mathbb{S}}(f^{(k-1)})]_{\mathtt{B},\mathtt{I}} & [L_{\mathbb{S}}(f^{(k-1)})]_{\mathtt{B},\mathtt{B}} \end{bmatrix} \begin{bmatrix} \mathbb{f}_{\mathtt{I}}^{(k)} \\ \mathbb{f}_{\mathtt{B}}^{(0)} \end{bmatrix} = \mathbf{0},$$

which is equivalent to (5.5).

(ii) As in Remark (ii) of Section 4, since the stretch energy functional $\mathcal{E}_{\mathbb{S}}(f)$ *in (5.1) is highly nonlinear and the condition* $|\tau| = |f(\tau)|$ *is imposed in (5.3) implicitly, the convergence of the VSEM Algorithm 5.1 for volume-preserving parameterizations are hard to be proved theoretically. For convergence criterion, it is reasonable to numerically check whether the resulting stretch factors* $\sigma_{f^{-1}}(\tau)$ *of (5.4) are close to one, as well as the volumetric stretch energy in (5.1) stop decreasing. The convergence of* $\mathcal{E}_{\mathbb{S}}(f)$ *and the distributions of* $\boldsymbol{\sigma}_{f^{-1}}(\tau)$ *for various benchmark mesh models are demonstrated in Figures 6.9 and 6.10, respectively. From Figure 6.9, it is expected that the convergence rate is sublinear and of* $O(1/k^s)$ *with* $1/2 \le s \le 1$.

(iii) In practice, the value of the stretch factor $\boldsymbol{\sigma}_{f^{-1}}(\tau)$ *in (5.4) could be extremely small which might potentially make the algorithm unstable. To remedy this drawback, we could add a global regularization constant* c *to* $\boldsymbol{\sigma}_{f^{-1}}(\tau)$ *at each iteration to make the algorithm much more reliable and efficient. In this case, the stretch factor* $\boldsymbol{\sigma}_{f^{-1}}(\tau)$ *in (5.4) is modified by*

$$\boldsymbol{\sigma}_{f^{-1}}(\tau) = \frac{|\tau|}{|f(\tau)|} + c, \;\; \tau \in \mathcal{T}(\mathcal{M}), \tag{5.6}$$

for some $c > 0$.

(iv) The bijectivity of the volume-preserving parameterization of genus-one tetrahedral meshes, in general, is not guaranteed even if the mapping is a convex combination with the boundary being convex. A counterexample has been given in [20]. The bijectivity of the volume-preserving parameterization can be checked by the number of flips of $\{f(\tau) \,|\, \tau \in \mathcal{T}(\mathcal{M})\}$. *See Tables 6.3 and 6.4 below.*

Algorithm 5.1 VSEM for Volume-Preserving Parameterizations

Input: A simply connected tetrahedral mesh $\mathcal{M}$ with $\partial\mathcal{M}$ being a genus-one closed surface, a tolerance ε (e.g. $\varepsilon = 10^{-6}$).

Output: A volume-preserving parameterization $\mathbb{f}$.

Let n be the number of vertices of $\mathcal{M}$.

Let $\mathtt{B} = \{s \,|\, v_s \in \partial\mathcal{M}\}$ and $\mathtt{I} = \{1, \ldots, n\}\backslash\mathtt{B}$.

Compute an area-preserving parameterization $\mathbb{g}_{\mathtt{B}}$ between $\partial\mathcal{M}$ and $\mathbb{T}^2$ by Algorithm 4.1.

Compute $\mathbb{g}$ by solving the linear system

$$[L_{\mathbb{D}}]_{\mathtt{I},\mathtt{I}}\mathbb{g}_{\mathtt{I}} = -[L_{\mathbb{D}}]_{\mathtt{I},\mathtt{B}}\mathbb{g}_{\mathtt{B}},$$

where $L_{\mathbb{D}} \in \mathbb{R}^{n\times n}$ is the volumetric Laplacian matrix [40, 41, 42] with

$$[L_{\mathbb{D}}]_{i,j} = \begin{cases} -w_{i,j} & \text{if } [v_i, v_j] \in \mathcal{E}(\mathcal{M}), \\ \sum_{k\neq i} w_{i,k} & \text{if } j = i, \\ 0 & \text{otherwise}, \end{cases} \tag{5.7}$$

in which $w_{i,j}$ is the cotangent weight on the edge $[v_i, v_j]$ given by

$$w_{i,j} = \frac{1}{6} \sum_{\substack{\tau\in\mathcal{T}(\mathcal{M}) \\ [v_i,v_j]\cup[v_k,v_\ell]\subset\tau \\ [v_i,v_j]\cap[v_k,v_\ell]=\varnothing}} |[v_k, v_\ell]| \cot\theta_{i,j}^{k,\ell}, \tag{5.8}$$

where $\theta_{i,j}^{k,\ell}$ is the dihedral angle between $[v_i, v_k, v_\ell]$ and $[v_j, v_\ell, v_k]$ in the tetrahedron τ on the edge $[v_k, v_\ell]$, as illustrated in Figure 5.1.

Set $\delta \leftarrow \infty$.

Set $\mathbb{f}_{\mathtt{B}} \leftarrow \mathbb{g}_{\mathtt{B}}$.

while $\delta > \varepsilon$ **do**

  Update $A \leftarrow L_{\mathbb{S}}(\mathbb{g})$, where $L_{\mathbb{S}}(\mathbb{g})$ is defined as in (5.2).

  Update $\mathbb{f}$ by solving the linear system $A_{\mathtt{I},\mathtt{I}}\mathbb{f}_{\mathtt{I}} = -A_{\mathtt{I},\mathtt{B}}\mathbb{f}_{\mathtt{B}}$.

  Update $\delta \leftarrow \mathcal{E}_{\mathbb{S}}(\mathbb{g}) - \mathcal{E}_{\mathbb{S}}(\mathbb{f})$.

  Update $\mathbb{g} \leftarrow \mathbb{f}$.

end while

return The volumetric mapping $\mathbb{f}$.

6. Numerical experiments.

In this section, we fist justify the holomorphic 1-form method [22, 23, 27] for the computation of the initial conformal map is better than the Ricci flow method [26, 48]. Then we demonstrate numerical experiments of the modified SEM algorithm for area-preserving mapping of genus-one closed triangular meshes and the VSEM algorithm for volume-preserving parameterizations of genus-one tetrahedral meshes. The linear systems in our algorithms are solved by the backslash operator (\) in MATLAB. The surface models, shown in Figures 6.1 and 7.2, are obtained from CGTrader [5], TurboSquid [2], AIM@SHAPE

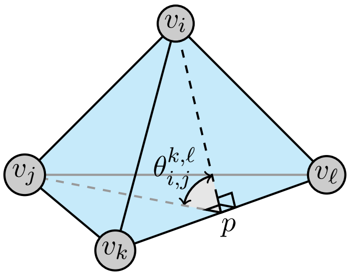

Figure 5.1. *An illustration for the dihedral angle between* $[v_i, v_k, v_\ell]$ *and* $[v_j, v_\ell, v_k]$ *in the tetrahedron* $[v_i, v_j, v_k, v_\ell]$.

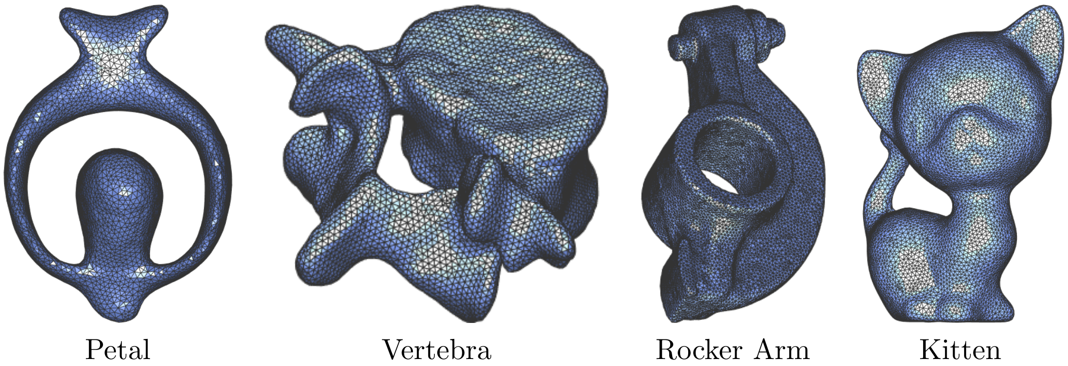

Figure 6.1. *The surface models of Petal, Vertebra, Rocker Arm, and Kitten.*

shape repository [1], Sketchfab [6] and Gu's website [4]. The tetrahedral meshes are generated using *JIGSAW* mesh generators [15, 18, 16, 19, 17].

6.1. Angle-preserving mappings of genus-one closed triangular meshes. In this subsection, we compare the conformality and the efficiency of the Ricci flow method [26, 48] and the holomorphic 1-form method [22, 23, 27] for the computation of the holomorphic map $z : \partial\mathcal{M} \to \mathbb{C}$ of genus-one closed surfaces that maps $\partial\mathcal{M}$ to its fundamental domain in $\mathbb{C}$. The conformality is measured by the conformal energy [25, 13] given by

$$\mathcal{E}_C(z) = \frac{1}{2}\mathbf{z}^* L\mathbf{z} - |z(\partial\mathcal{M})|, \tag{6.1}$$

where L is the cotangent-weighted Laplacian matrix. The Ricci flow method is performed by the software `RicciFlow` developed by Gu [7].

From Table 6.1, we see that the resulting mapping by the holomorphic 1-form method [22, 23, 27] has slightly better accuracy in terms of conformal energy, and significantly better efficiency, compared to the Ricci flow method [26, 48]. Therefore, we adapt the holomorphic 1-form method, summarized in Algorithm 3.1, as the method for computing the initial conformal mapping in Algorithm 4.1.

6.2. Area-preserving mappings of genus-one closed triangular meshes. We now introduce the distortion measurements of the accuracy of an area-preserving mapping $g : \partial\mathcal{M} \to \mathbb{T}^2$.

Table 6.1

The conformal energy $\mathcal{E}_C$ and the execution time cost (sec.) of angle-preserving mapping by the Ricci flow method [26, 48] and the holomorphic 1-form method [22, 23, 27] (Algorithm 3.1). $\#\mathcal{F}(\partial\mathcal{M})$ denotes the number of triangular faces of the model.

Model Name	$\#\mathcal{F}(\partial\mathcal{M})$	Ricci Flow		Holomorphic 1-Form	
		$\mathcal{E}_C$	Time	$\mathcal{E}_C$	Time
Petal	14,506	2.6773×10^{-3}	2.10	2.4208×10^{-3}	0.39
Vertebra	16,420	2.0765×10^{-3}	2.45	2.0385×10^{-3}	0.44
Rocker Arm	25,182	3.7663×10^{-4}	4.07	3.6363×10^{-4}	0.70
Kitten	21,584	1.8736×10^{-3}	3.18	1.8056×10^{-3}	0.56

The global area distortion of the mapping g is measured by the *total area distortion* defined as

$$\mathcal{D}_{\text{area}}(g) = \frac{1}{4} \sum_{v\in\mathcal{V}(\partial\mathcal{M})} \left| \frac{\sum_{\tau\in\mathcal{N}_{\mathcal{F}}(v)} |\tau|}{|\partial\mathcal{M}|} - \frac{\sum_{\tau\in\mathcal{N}_{\mathcal{F}}(v)} |g(\tau)|}{|g(\partial\mathcal{M})|} \right|, \tag{6.2}$$

where $\mathcal{N}_{\mathcal{F}}(v) = \{\tau \in \mathcal{F}(\partial\mathcal{M}) \,|\, v \subset \tau\}$ is the set of neighboring triangular faces of the vertex v, $|\partial\mathcal{M}|$ and $|f(\partial\mathcal{M})|$ denote areas of $\partial\mathcal{M}$ and its image, respectively. The mapping g is area-preserving if $\mathcal{D}_{\text{area}}(g) = 0$. In addition, the local area distortion of the mapping g is measured by the mean and standard deviation (SD) of the *local area ratios* defined as

$$\mathcal{R}_{\text{area}}(g, v) = \frac{\sum_{\tau\in\mathcal{N}_{\mathcal{F}}(v)} |g(\tau)|/|g(\partial\mathcal{M})|}{\sum_{\tau\in\mathcal{N}_{\mathcal{F}}(v)} |\tau|/|\partial\mathcal{M}|}. \tag{6.3}$$

Also, the mapping g is area-preserving if the mean is 1 and the SD is 0.

Figures 6.2 to 6.5 show the boundaries of four tetrahedral mesh models, their equiareal mapping on $\mathbb{T}^2$ and the associated fundamental domain computed by the modified SEM Algorithm 4.1.

Figure 6.6 shows the relationship between the number of iterations and the stretch energy as well as the total area distortion of the area-preserving mapping computed by the modified SEM Algorithm 4.1. It is worth mentioning that both the stretch energy and the total area distortion are significantly decreased in the first 5 iteration steps, and monotonically decreasing during the whole iteration procedure, which indicates that the modified SEM algorithm works effectively on reducing both the stretch energy and the total area distortion.

Table 6.2 shows the total area distortion, the mean and SD of local area ratios, and the number of overlapped triangular faces computed by Algorithm 4.1. We observe that the total area distortions of four mappings are between 1%-5%. In addition, the means of the local area ratios are close to 1 with fairly small SDs, and the corresponding histograms of local area ratios are presented in Figure 6.7. These imply that the mappings preserve the local area well. Furthermore, it is worth noting that all resulting mappings are bijective.

6.3. Volume-preserving parameterizations of genus-one tetrahedral meshes. We now introduce the distortion measurement of the accuracy of a volume-preserving parameterization

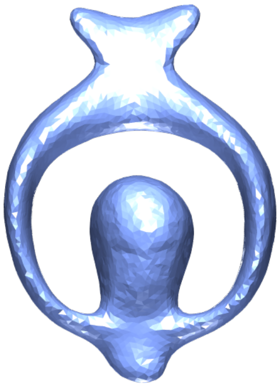

The boundary of Petal

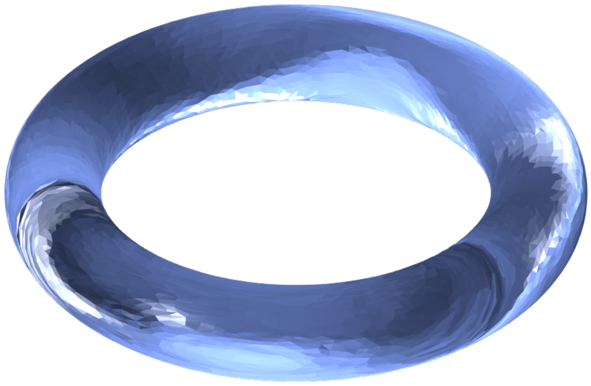

The torus mapping of Petal

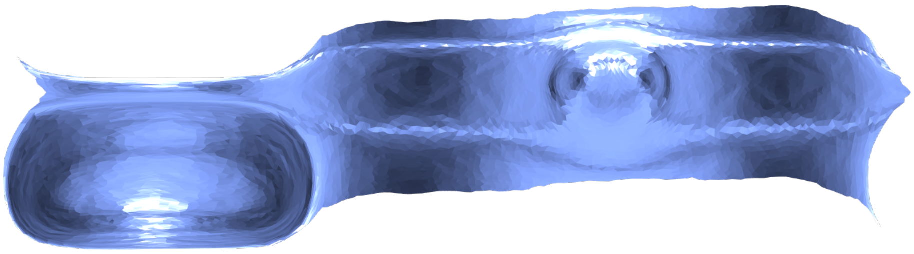

The fundamental domain of Petal

Figure 6.2. *The boundary of the tetrahedral mesh model Petal and its area-preserving parameterization on $\mathbb{T}^2$ as well as the associated fundamental domain computed by the modified SEM Algorithm 4.1.*

Table 6.2

The total area distortion $\mathcal{D}_{area}$ as well as the mean and SD of local area ratios $\mathcal{R}_{area}$ of area-preserving mapping by the SEM Algorithm 4.1. $\#\mathcal{F}(\partial\mathcal{M})$ denotes the number of triangular faces of the model.

Model Name	$\#\mathcal{F}(\partial\mathcal{M})$	$\mathcal{D}_{\text{area}}$	$\mathcal{R}_{\text{area}}$		#Flip
			Mean	SD	
Petal	14,506	0.0169	1.0000	0.0288	0
Vertebra	16,420	0.0201	0.9999	0.0367	0
Rocker Arm	25,182	0.0119	1.0001	0.0200	0
Kitten	21,584	0.0465	1.0006	0.0999	0

$f : \mathcal{M} \to \mathbb{T}^3$. The global volume distortion of the mapping f is measured using the *total volume distortion* defined as

$$\mathcal{D}_{\text{volume}}(f) = \frac{1}{4} \sum_{v \in \mathcal{V}(\mathcal{M})} \left| \frac{\sum_{\tau \in \mathcal{N}_{\mathcal{T}}(v)} |\tau|}{|\mathcal{M}|} - \frac{\sum_{\tau \in \mathcal{N}_{\mathcal{T}}(v)} |f(\tau)|}{|f(\mathcal{M})|} \right|, \tag{6.4}$$

where $\mathcal{N}_{\mathcal{T}}(v) = \{\tau \in \mathcal{T}(\mathcal{M}) \,|\, v \subset \tau\}$ is the set of neighboring tetrahedrons of the vertex v, $|\mathcal{M}|$ and $|f(\mathcal{M})|$ denote volumes of $\mathcal{M}$ and its image, respectively. The mapping f is volume-preserving if $\mathcal{D}_{\text{volume}}(f) = 0$. In addition, the local volume distortion of the mapping f is

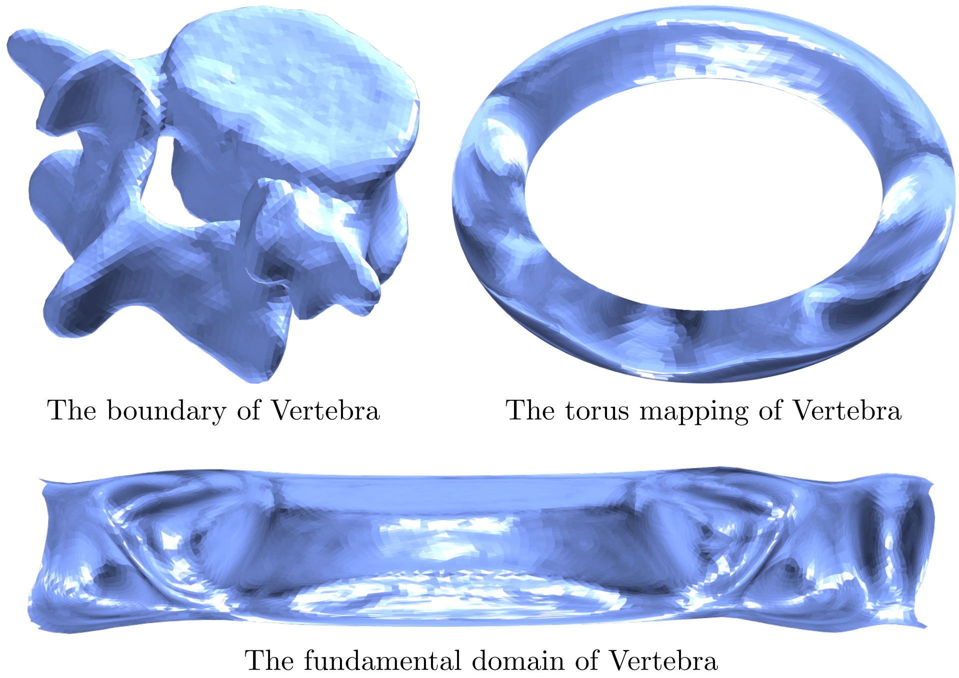

Figure 6.3. *The boundary of the tetrahedral mesh model Vertebra and its area-preserving parameterization on $\mathbb{T}^2$ as well as the associated fundamental domain computed by the modified SEM Algorithm 4.1.*

measured by the mean and SD of the *local volume ratios* defined as

$$\mathcal{R}_{\text{volume}}(f, v) = \frac{\sum_{\tau\in\mathcal{N}_{\mathcal{T}}(v)} |f(\tau)|/|f(\mathcal{M})|}{\sum_{\tau\in\mathcal{N}_{\mathcal{T}}(v)} |\tau|/|\mathcal{M}|}. \tag{6.5}$$

Also, the mapping f is volume-preserving if the mean is 1 and the SD is 0.

Figure 6.8 shows the tetrahedral mesh model Vertebra and its volume-preserving parameterization computed by the VSEM Algorithm 5.1.

Figure 6.9 shows the relationship between the number of iterations and the volumetric stretch energy as well as the total volume distortion of the parameterization computed by the VSEM Algorithm 5.1. We observe that both of the volumetric stretch energy and the total volume distortion are significantly decreased in the first 20 iterations, and monotonically decreasing during the whole iteration procedure, which shows that the VSEM algorithm works effectively on reducing both the volumetric stretch energy and the total volume distortion of the parameterization.

Table 6.3 shows the relationship between the regularization constant c as in (5.6), the total volume distortion, the local volume ratios, and the number of flipped tetrahedrons of the parameterization computed by the VSEM Algorithm 5.1. We observe that the bijectivity of the parameterization can be improved by increasing the value of the regularization constant c and slightly sacrificing the total and local volume distortion.

In Table 6.4, we show numbers of iterations of volume-preserving parameterizations for various genus-one tetrahedral models computed by the modified VSEM Algorithm 5.1 with

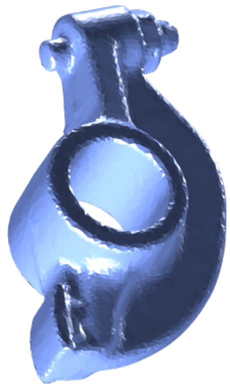

The boundary of Rocker Arm

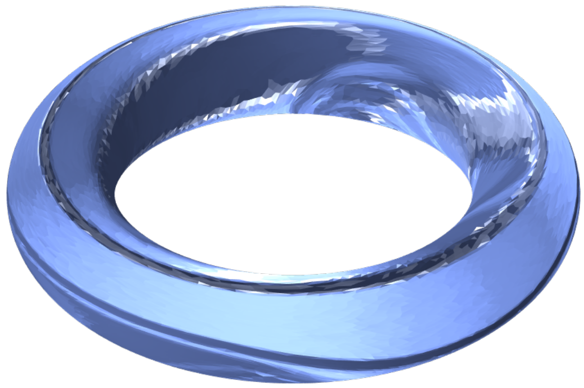

The torus mapping of Rocker Arm

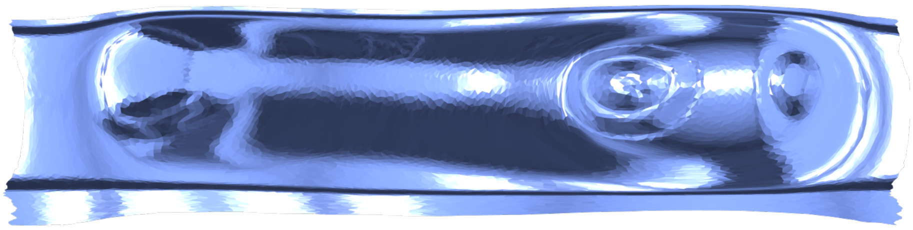

The fundamental domain of Rocker Arm

Figure 6.4. *The boundary of the tetrahedral mesh model Rocker Arm and its area-preserving parameterization on $\mathbb{T}^2$ as well as the associated fundamental domain computed by the modified SEM Algorithm 4.1.*

the regularization constant $c = 10$ vs. the total volume and local volume (mean and SD) distortions as well as the number of flipped tetrahedrons. In practice, the VSEM Algorithm 5.1 begins with the harmonic map of $L_{\mathbb{D}}$ in (5.7) with the fixed boundary $\mathrm{g}_{\mathtt{B}}$ given in Step 3. For four cases we see that after 20 iterations, the means are close to 1 ± 0.02, the SDs significantly reduce from $(0.7348, 0.7508, 0.7041, 0.8085)$ to $(0.5257, 0.4895, 0.3887, 0.4790)$, respectively, as well as the numbers of flipped tetrahedrons reduce from 656 (99.36%), 9109 (95.04%), 670 (99.71%) and 5081 (98.57%) to 14 (99.99%), 0 (100%), 14 (99.99%) and 30 (99.99%), respectively, which are rather satisfactory in practical applications.

Figure 6.10 shows the histogram of the local volume ratios of the four models. We observe that the ratios of Petal and Kitten seemingly form binomial distributions with two local means, respectively, less and greater than one. In Figure 6.1 we see that the parts with larger surfaces, such as the "bud" of Petal and the "head" of Kitten have local means slightly smaller than one, while the other parts with smaller surfaces have local means greater than one. However, the means of local volume ratios are quite close to one as shown in Table 6.4.

7. Applications.

In this section, we present applications of volume-preserving parameterizations for genus-one 3-manifolds on Vertebra registrations and partitions.

7.1. Vertebra registrations.

A Vertebra is a 3-manifold with the boundary being a genus-one closed surface. Given a pair of Vertebrae $\mathcal{M}$ and $\mathcal{N}$ with n landmarks $\{p_\ell\}_{\ell=1}^n \subset \partial\mathcal{M}$ and $\{q_\ell\}_{\ell=1}^n \subset \partial\mathcal{N}$, respectively. The aim of the Vertebrae registration is to find a volume-

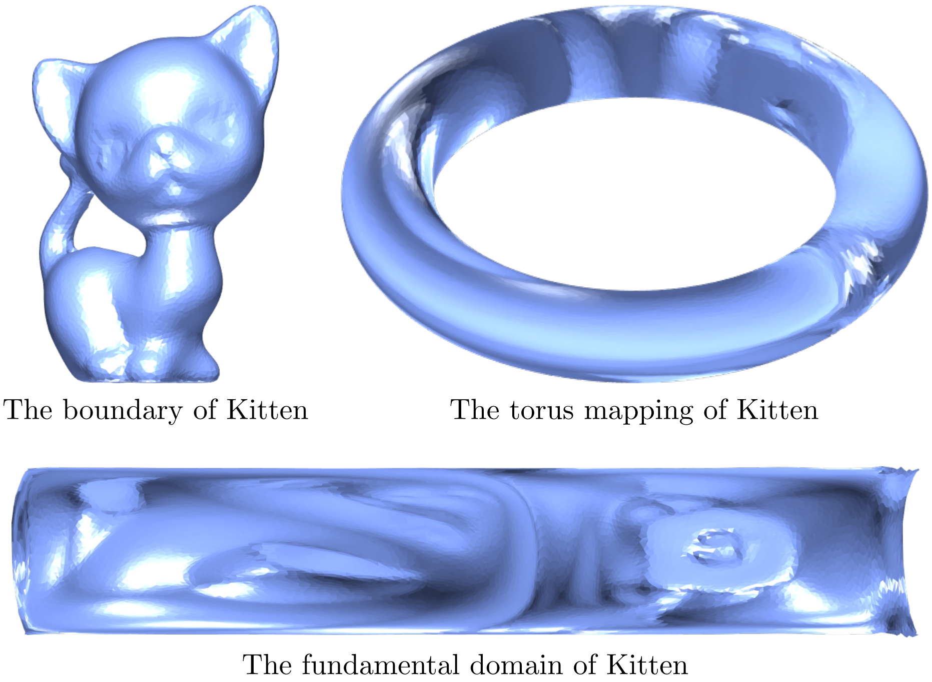

Figure 6.5. *The boundary of the tetrahedral mesh model Kitten and its area-preserving parameterization on $\mathbb{T}^2$ as well as the associated fundamental domain computed by the modified SEM Algorithm 4.1.*

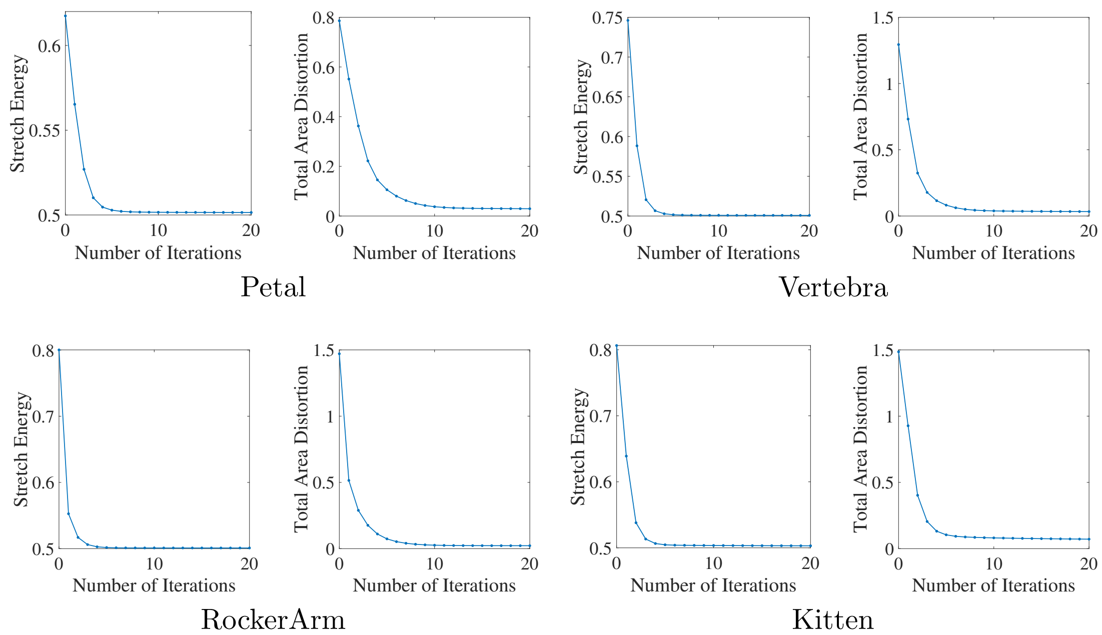

Figure 6.6. *The relationship between the number of iterations and the stretch energy as well as the total area distortion of the area-preserving parameterizations computed by the modified SEM Algorithm 4.1.*

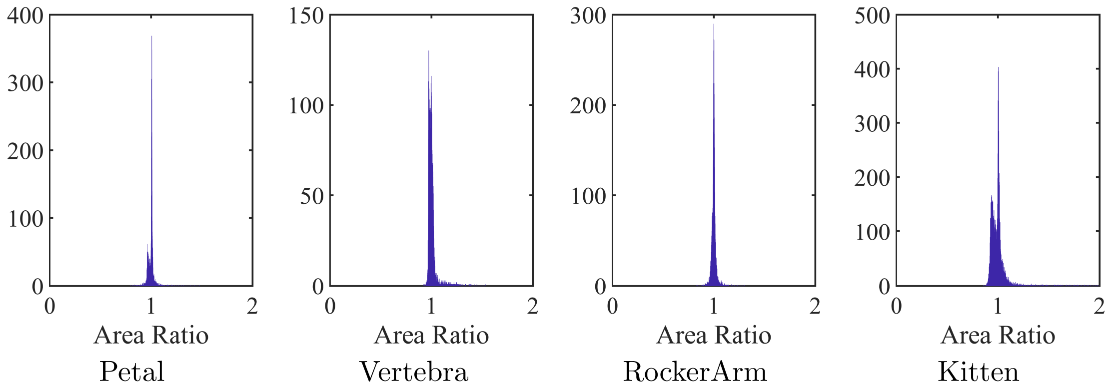

Figure 6.7. *Histogram of local area ratios of the torus parameterization computed by the modified SEM Algorithm 4.1.*

Table 6.3

The total volume distortion $\mathcal{D}_{volume}$ as well as the mean and SD of local volume ratios $\mathcal{R}_{volume}$ of volume-preserving parameterizations by the VSEM algorithm. $\#\mathcal{T}(\mathcal{M})$ denotes the number of tetrahedrons of the model, and c is the regularization constant. The maximal number of iterations is 20.

Model Name $\#\mathcal{T}(\mathcal{M})$	c	$\mathcal{D}_{\text{volume}}$	$\mathcal{R}_{\text{volume}}$ Mean	$\mathcal{R}_{\text{volume}}$ SD	#Flip	Bijectivity (%)	Time (sec.)
Petal 102,513	0	0.2751	1.0284	0.3513	504	99.51%	11.67
	1	0.2945	1.0320	0.3957	198	99.81%	11.45
	10	0.3862	1.0281	0.5257	14	99.99%	11.38
Vertebra 183,792	0	0.3227	1.0180	0.3710	49	99.97%	19.56
	1	0.3401	1.0192	0.3943	7	100.00%	19.58
	10	0.3879	1.0228	0.4895	0	100.00%	19.74
Rocker Arm 227,216	0	0.0960	1.0059	0.1472	583	99.74%	25.46
	1	0.1277	1.0108	0.2037	216	99.90%	25.46
	10	0.2818	1.0112	0.3887	14	99.99%	25.40
Kitten 354,772	0	0.1440	1.0053	0.2018	373	99.89%	39.71
	1	0.1748	1.0106	0.2585	161	99.95%	39.85
	10	0.2875	1.0289	0.4790	30	99.99%	39.94

preserving mapping $f : \mathcal{M} \to \mathcal{N}$ such that $f(p_\ell) = q_\ell$, for $\ell = 1, \ldots, n$.

First, the boundaries $\partial\mathcal{M}$ and $\partial\mathcal{N}$ of the Vertebrae are mapped holomorphically to their fundamental domains by

$$\varphi : \partial\mathcal{M} \to \mathbb{C} \quad \text{and} \quad \psi : \partial\mathcal{N} \to \mathbb{C},$$

respectively, using Algorithm 3.1, as illustrated in Figure 7.1. Let $c_1, \ldots, c_4$ and $d_1, \ldots, d_4$ counterclockwise be four corner points of the fundamental domains $\varphi(\partial\mathcal{M})$ and $\psi(\partial\mathcal{N})$, respectively. The size of $\varphi(\partial\mathcal{M})$ is normalized by an affine transformation $\alpha : \mathbb{C} \to \mathbb{C}$ that satisfies

$$\alpha \circ \varphi(c_\ell) = \psi(d_\ell), \quad \text{for } \ell = 1, \ldots, 4.$$

Then a coarse Delaunay triangular mesh $\mathcal{P}$ of the points $\{\alpha \circ \varphi(p_\ell)\}_{\ell=1}^n \cup \{\alpha \circ \varphi(c_\ell)\}_{\ell=1}^4$ is

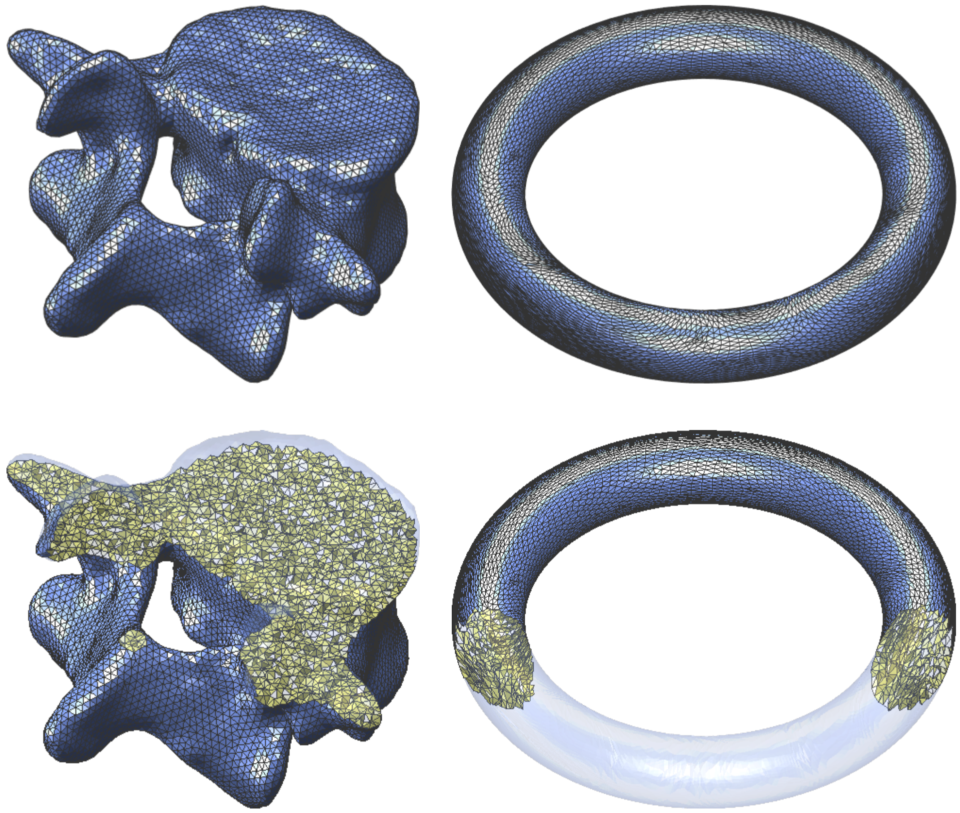

Figure 6.8. *The tetrahedral mesh model Vertebra and its volume-preserving parameterization computed by the VSEM Algorithm* 5.1.

generated on $\mathbb{C}$ using the function `delaunay` in MATLAB. Note that $\mathcal{P}$ is a mesh of the rectangle with the vertices

$$\mathcal{V}(\mathcal{P}) = \{\alpha \circ \varphi(p_\ell)\}_{\ell=1}^n \cup \{\alpha \circ \varphi(c_\ell)\}_{\ell=1}^4.$$

Let $\mathcal{Q}$ be the triangular mesh of the vertices

$$\mathcal{V}(\mathcal{Q}) = \{\psi(q_\ell)\}_{\ell=1}^n \cup \{\psi(d_\ell)\}_{\ell=1}^4$$

with the same vertex adjacency as $\mathcal{P}$. Then a piecewise affine mapping $h : \mathcal{P} \to \mathcal{Q}$ is induced by mapping each triangular face in $\mathcal{F}(\mathcal{P})$ to the corresponding triangular face in $\mathcal{F}(\mathcal{Q})$ using the barycentric coordinates of the triangles. The boundary registration mapping $g : \partial\mathcal{M} \to \partial\mathcal{N}$ is then given by

$$g = \psi^{-1} \circ h \circ \alpha \circ \varphi.$$

Ultimately, the volume-preserving mapping $f : \mathcal{M} \to \mathcal{N}$ is computed using Algorithm 5.1 with the boundary mapping $f|_{\partial\mathcal{M}}$ in Step 3 being g.

In practice, the considered Vertebrae $\mathcal{M}$ and $\mathcal{N}$ are the tetrahedral meshes Vertebra 1 and Vertebra 2 with 38 landmarks on the boundaries, respectively, as shown in Figure 7.1. The

Table 6.4

The relationship between the number of iterations and the volumetric stretch energy as well as the total volume distortion $\mathcal{D}_{volume}$ and the local volume ratio $\mathcal{R}_{volume}$ of volume-preserving parameterizations by the VSEM algorithm with the regularization constant $c = 10$. $\#\mathcal{T}(\mathcal{M})$ denotes the number of tetrahedrons of the model.

Model Name $\#\mathcal{T}(\mathcal{M})$	#Iter.	$E_{\mathbb{S}}$	$\mathcal{D}_{\text{volume}}$	$\mathcal{R}_{\text{volume}}$ Mean	$\mathcal{R}_{\text{volume}}$ SD	#Flip	Bijectivity (%)	Time (sec.)
Petal 102,513	0	3.1305	0.5859	1.0014	0.7348	656	99.36	11.38
	1	3.1241	0.5664	1.0046	0.7152	209	99.80	
	5	3.1166	0.5045	1.0141	0.6517	37	99.96	
	10	3.1137	0.4514	1.0212	0.5955	19	99.98	
	20	3.1115	0.3862	1.0281	0.5257	14	99.99	
Vertebra 183,792	0	0.0827	0.6092	1.0107	0.7508	9109	95.04	19.74
	1	0.0818	0.5922	1.0142	0.7299	518	99.72	
	5	0.0814	0.5136	1.0203	0.6385	3	100.00	
	10	0.0813	0.4500	1.0228	0.5657	0	100.00	
	20	0.0812	0.3879	1.0228	0.4895	0	100.00	
Rocker Arm 227,216	0	7.0445	0.5650	0.9734	0.7041	670	99.71	25.40
	1	7.0297	0.5380	0.9780	0.6719	304	99.87	
	5	7.0123	0.4505	0.9912	0.5712	41	99.98	
	10	7.0054	0.3734	1.0012	0.4860	15	99.99	
	20	7.0003	0.2818	1.0112	0.3887	14	99.99	
Kitten 354,772	0	3.2989	0.5392	1.0612	0.8085	5081	98.57	39.94
	1	3.2888	0.5123	1.0583	0.7770	120	99.97	
	5	3.2789	0.4288	1.0482	0.6746	24	99.99	
	10	3.2757	0.3607	1.0394	0.5867	23	99.99	
	20	3.2737	0.2875	1.0289	0.4790	30	99.99	

total volume distortion of the resulting volume-preserving mapping $f : \mathcal{M} \to \mathcal{N}$ is 0.0739, and the mean and SD of the volume ratios are 0.9944 and 0.1214, respectively. The histogram of volume ratios of the mapping f, shown in Figure 7.1, indicates that most of the volume ratios are concentrated at 1, which is quite satisfactory. The evolution of deformation between the Vertebrae by the linear homotopy method can be found at https://mhyueh.github.io/projects/Torus_VSEM.html.

7.2. Volume-based manifold partitions. The volume-based manifold partition refers to separating a manifold into several parts according to the volume. With aid of the VSEM Algorithm 5.1, a manifold $\mathcal{M}$ can be mapped to the standard solid torus $\mathbb{T}^3$ by $f : \mathcal{M} \to \mathbb{T}^3$ with fairly small volume distortion. Note that $\mathbb{T}^3$ can be parameterized by the mapping $\xi : [0, 2\pi) \times [0, 2\pi) \times [0, r] \to \mathbb{T}^3$ defined as

$$\xi(u, v, s) = ((R + s\cos v)\cos u, (R + s\cos v)\sin u, s\sin v)\,, \tag{7.1}$$

where r is the radius of the tube, R is the distance from the center of the tube to the center of the torus, and $u, v \in [0, 2\pi)$, $s \in [0, r]$. The partition of $\mathbb{T}^3$ can then be selected by

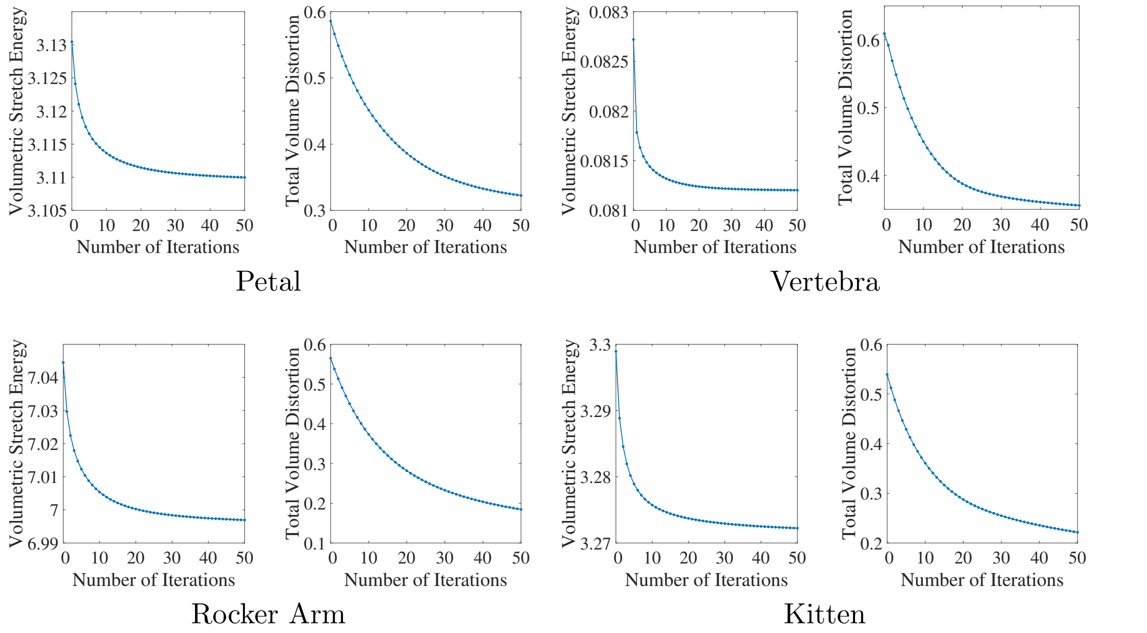

Figure 6.9. *The relationship between the number of iterations and the volumetric stretch energy as well as the total volume distortion of the parameterization computed by the VSEM Algorithm* 5.1.

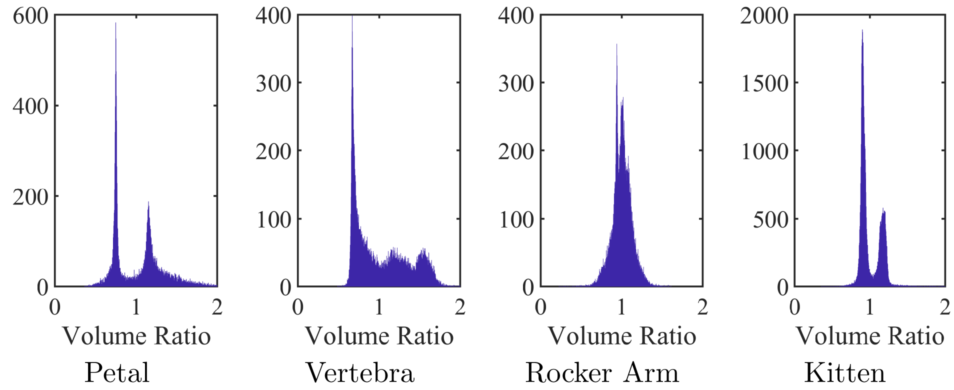

Figure 6.10. *Histogram of the local volume ratios of the parameterizations computed by the VSEM Algorithm* 5.1.

the parameters u, v, s of the map ξ. Suppose a submanifold $\mathcal{S}$ of $\mathbb{T}^3$ is selected. Then the corresponding partition $\widehat{\mathcal{M}} \equiv f^{-1}(\mathcal{S}) \subset \mathcal{M}$ can be easily constructed by the inverse map $f^{-1} : \mathbb{T}^3 \to \mathcal{M}$.

In practice, we consider the Vertebra tetrahedral mesh model $\mathcal{M}$ shown in Figure 6.8. First, a volume-preserving mapping $f : \mathcal{M} \to \mathbb{T}^3$ between $\mathcal{M}$ and $\mathbb{T}^3$ is computed by the VSEM Algorithm 5.1. Then, a uniform sampling $\mathcal{V}(\mathbb{T}^3)$ of $\mathbb{T}^3$ is constructed using the parameterization $\xi(u, v, s)$ in (7.1) so that the size of each part can be easily controlled by parameters u, v, s. The tetrahedral mesh $\mathcal{T}(\mathbb{T}^3)$ of the sampling $\mathcal{V}(\mathbb{T}^3)$ can be constructed by applying the functions `alphaShape` and `alphaTriangulation` in MATLAB. Next, we selected a part

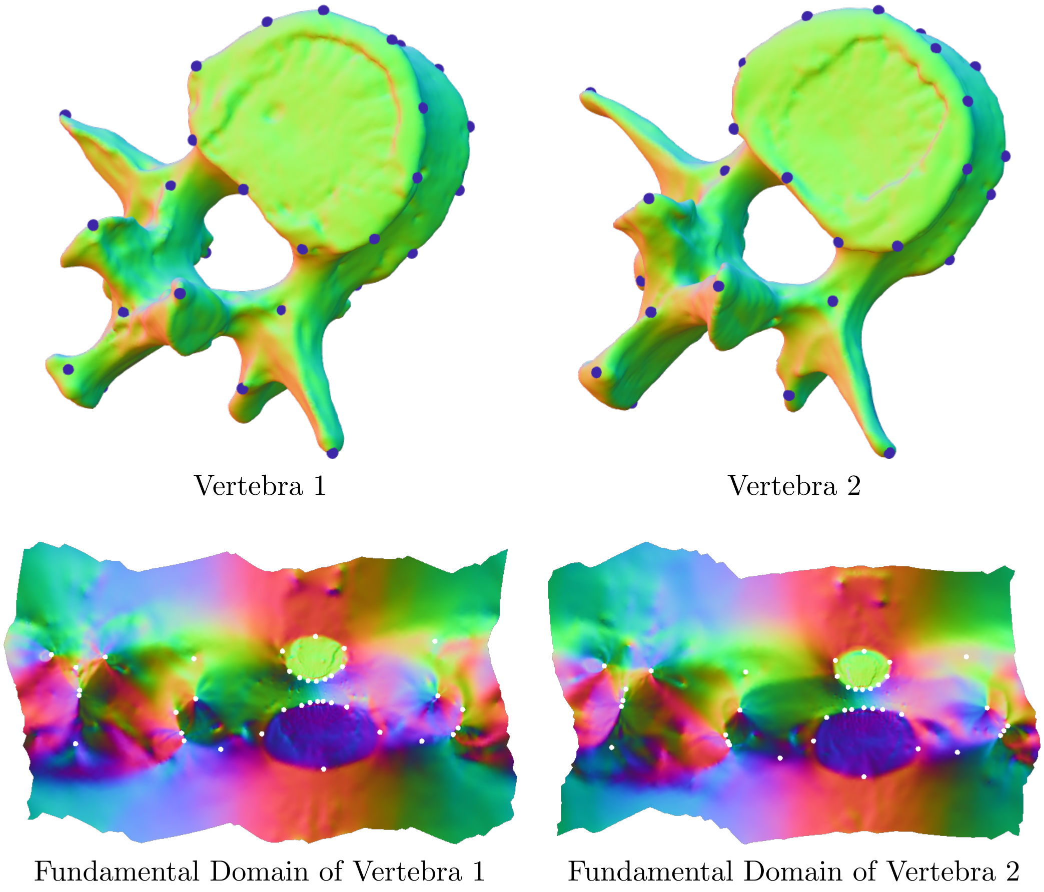

Figure 7.1. *The boundaries of the tetrahedral mesh model Vertebra 1 and Vertebra 2 as well as their fundamental domains.*

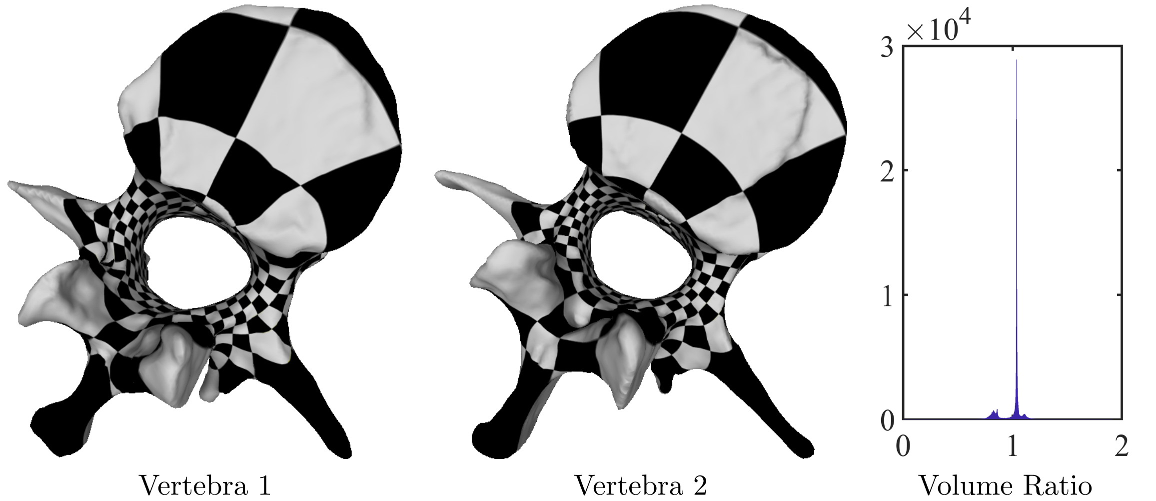

Figure 7.2. *The charts of the boundaries of the tetrahedral mesh model Vertebra 1 and Vertebra 2 and the histogram of volume ratios of the registration mapping.*

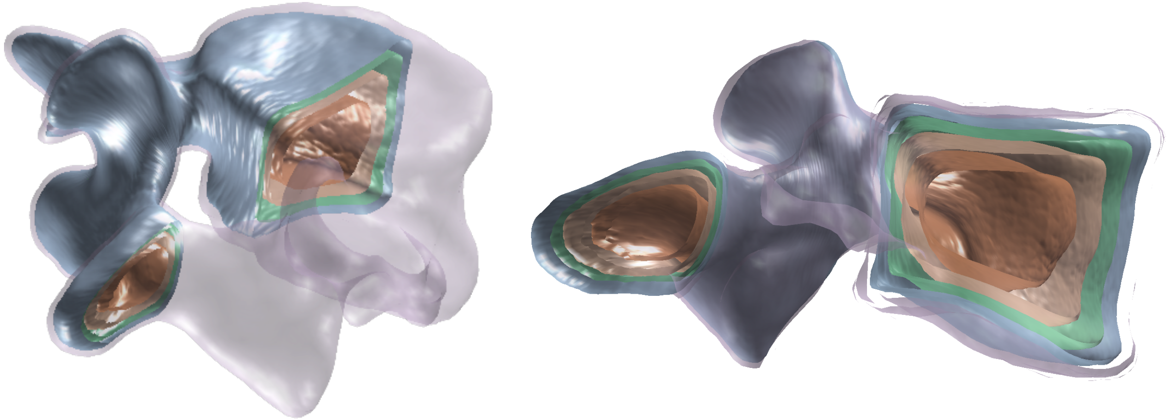

Figure 7.3. *The level surfaces of Vertebra with volumes being $\frac{1}{5}, \frac{2}{5}, \frac{3}{5}, \frac{4}{5}$ the volume of Vertebra, endowed by colors (red, orange, green, blue), respectively.*

Table 7.1
The volume ratios $\frac{|\widehat{\mathcal{M}}_k|}{|\mathcal{M}|}$ and the relative errors $\frac{\left||\widehat{\mathcal{M}}_k|-\frac{k}{5}|\mathcal{M}|\right|}{\frac{k}{5}|\mathcal{M}|}$ of the submanifold $\widehat{\mathcal{M}}_k$, for $k = 1, 2, 3, 4$.

k	1	2	3	4
Volume Ratio $\frac{|\widehat{\mathcal{M}}_k|}{|\mathcal{M}|}$	0.1998	0.3998	0.6010	0.8012
Relative Error $\frac{\left||\widehat{\mathcal{M}}_k|-\frac{k}{5}|\mathcal{M}|\right|}{\frac{k}{5}|\mathcal{M}|}$	0.08%	0.06%	0.17%	0.15%

of $\mathbb{T}^3$ by

$$\mathcal{S}_k \equiv \xi\left([0, 2\pi) \times [0, 2\pi) \times \left[0, \sqrt{\frac{k}{5}}r\right]\right),$$

with the volume being $\frac{k}{5}|\mathbb{T}^3|$, for $k = 1, 2, 3, 4$. Ultimately, the corresponding submanifold $\widehat{\mathcal{M}}_k$ in $\mathcal{M}$ is constructed by

$$\widehat{\mathcal{M}}_k \equiv f^{-1}(\mathcal{S}_k).$$

In Figure 7.3, we show the level surfaces of the submanifolds $\widehat{\mathcal{M}}_k$ of Vertebra with volumes being $\frac{1}{5}, \frac{2}{5}, \frac{3}{5}, \frac{4}{5}$ of the volume of Vertebra, endowed by colors (red, orange, green, blue), respectively. In Table 7.1, we see that the volume ratios $\frac{|\widehat{\mathcal{M}}_k|}{|\mathcal{M}|}$ is quite close to $\frac{k}{5}$, for $k = 1, 2, 3, 4$, and the relative errors $\frac{\left||\widehat{\mathcal{M}}_k|-\frac{k}{5}|\mathcal{M}|\right|}{\frac{k}{5}|\mathcal{M}|}$ are less than 0.17%, which are fairly acceptable.

8. Concluding remarks. In this paper, we develop novel algorithms for the minimization of the stretch and volumetric stretch energies, which can be used to compute the angle- and area-preserving parameterizations of topological tori, as well as, the volume-preserving parameterizations of topological solid tori, respectively. Numerical experiments indicate that both SEM and VSEM algorithms perform well on practical models. Applications of the Vertebrae registrations and the volume-based manifold partitions are demonstrated to show the robustness of our algorithms.

REFERENCES

[1] *Digital Shape Workbench - Shape Repository*. http://visionair.ge.imati.cnr.it/ontologies/shapes/. (2016).

[2] *TurboSquid*. http://www.turbosquid.com/. (2016).

[3] *ReebHanTun Software*. http://web.cse.ohio-state.edu/~dey.8/handle/ReebHanTun-download/reebhantun.html, (2013).

[4] *David Xianfeng Gu's Home Page*. http://www3.cs.stonybrook.edu/~gu/, (2017).

[5] *CGTrader*. https://www.cgtrader.com/, (2019).

[6] *Sketchfab*. https://sketchfab.com/, (2019).

[7] *RiemannMapper : A Mesh Parameterization Toolkit*. https://www3.cs.stonybrook.edu/~gu/software/RiemannMapper/index.html, (2020).

[8] A. Chern, U. Pinkall, and P. Schröder, *Close-to-conformal deformations of volumes*, ACM Trans. Graph., 34 (2015), pp. 56:1–56:13, https://doi.org/10.1145/2766916.

[9] G. P.-T. Choi and L. M. Lui, *A linear formulation for disk conformal parameterization of simply-connected open surfaces*, Adv. Comput. Math., (2017), pp. 1–28, https://doi.org/10.1007/s10444-017-9536-x.

[10] G. P. T. Choi and C. H. Rycroft, *Density-equalizing maps for simply connected open surfaces*, SIAM J. Imaging Sci., 11 (2018), pp. 1134–1178, https://doi.org/10.1137/17M1124796.

[11] P. T. Choi, K. C. Lam, and L. M. Lui, *FLASH: Fast landmark aligned spherical harmonic parameterization for genus-0 closed brain surfaces*, SIAM J. Imaging Sci., 8 (2015), pp. 67–94, https://doi.org/10.1137/130950008.

[12] P. T. Choi and L. M. Lui, *Fast disk conformal parameterization of simply-connected open surfaces*, J. Sci. Comput., 65 (2015), pp. 1065–1090, https://doi.org/10.1007/s10915-015-9998-2.

[13] M. Desbrun, M. Meyer, and P. Alliez, *Intrinsic parameterizations of surface meshes*, Comput. Graph. Forum, 21 (2002), pp. 209–218.

[14] T. K. Dey, K. Li, J. Sun, and D. Cohen-Steiner, *Computing geometry-aware handle and tunnel loops in 3d models*, ACM Trans. Graph., 27 (2008), pp. 45:1–45:9, https://doi.org/10.1145/1360612.1360644.

[15] D. Engwirda, *Locally optimal Delaunay-refinement and optimisation-based mesh generation*, PhD thesis, University of Sydney, 2014, http://hdl.handle.net/2123/13148.

[16] D. Engwirda, *Voronoi-based point-placement for three-dimensional delaunay-refinement*, Procedia Engineering, 124 (2015), pp. 330–342, https://doi.org/10.1016/j.proeng.2015.10.143. 24th International Meshing Roundtable.

[17] D. Engwirda, *Conforming restricted delaunay mesh generation for piecewise smooth complexes*, Procedia Engineering, 163 (2016), pp. 84–96, https://doi.org/10.1016/j.proeng.2016.11.024. 25th International Meshing Roundtable.

[18] D. Engwirda and D. Ivers, *Face-centred voronoi refinement for surface mesh generation*, Procedia Engineering, 82 (2014), pp. 8–20, https://doi.org/10.1016/j.proeng.2014.10.364. 23rd International Meshing Roundtable (IMR23).

[19] D. Engwirda and D. Ivers, *Off-centre steiner points for delaunay-refinement on curved surfaces*, Computer-Aided Design, 72 (2016), pp. 157–171, https://doi.org/10.1016/j.cad.2015.10.007. 23rd International Meshing Roundtable Special Issue: Advances in Mesh Generation.

[20] M. S. Floater and V. Pham-Trong, *Convex combination maps over triangulations, tilings, and tetrahedral meshes*, Advances in Computational Mathematics, 25 (2006), pp. 347–356, https://doi.org/10.1007/s10444-004-7620-5.

[21] X. Gu, F. Luo, J. Sun, and S.-T. Yau, *Variational principles for Minkowski type problems, discrete optimal transport, and discrete Monge-Ampère equations*, Asian J. Math., 20 (2016), pp. 383–398, https://doi.org/10.4310/AJM.2016.v20.n2.a7.

[22] X. Gu and S.-T. Yau, *Computing conformal structures of surfaces*, Communications in Information and Systems, 2 (2002), pp. 121–146, https://doi.org/10.4310/CIS.2002.v2.n2.a2.

[23] X. Gu and S.-T. Yau, *Global conformal surface parameterization*, in Eurographics Symposium on Geometry Processing, L. Kobbelt, P. Schroeder, and H. Hoppe, eds., SGP '03, 2003, pp. 127–137, http://dl.acm.org/citation.cfm?id=882370.882388.

[24] X. Gu and S.-T. Yau, *Computational Conformal Geometry*, Higher Education Press, 1 ed., 2008.

[25] J. E. Hutchinson, *Computing conformal maps and minimal surfaces*, Proc. Centre Math. Appl., 26 (1991), pp. 140–161.

[26] M. Jin, J. Kim, F. Luo, and X. Gu, *Discrete surface ricci flow*, IEEE Trans. Vis. Comput. Graphics, 14 (2008), pp. 1030–1043, https://doi.org/10.1109/TVCG.2008.57.

[27] M. Jin, Y. Wang, S.-T. Yau, and X. Gu, *Optimal global conformal surface parameterization*, in IEEE Visualization 2004, Oct. 2004, pp. 267–274, https://doi.org/10.1109/VISUAL.2004.75.

[28] Y. Jin, G.-P. Qian, J.-Y. Zhao, J. Chang, R.-F. Tong, and J. Zhang, *Stretch-minimizing volumetric parameterization*, J. Comput. Sci. Tech-Ch., 30 (2015), pp. 553–564, https://doi.org/10.1007/s11390-015-1545-y.

[29] S. Z. Kovalsky, N. Aigerman, R. Basri, and Y. Lipman, *Controlling singular values with semidefinite programming*, ACM Trans. Graph., 33 (2014), pp. 68:1–68:13, https://doi.org/10.1145/2601097.2601142.

[30] S. Z. Kovalsky, N. Aigerman, R. Basri, and Y. Lipman, *Large-scale bounded distortion mappings*, ACM Trans. Graph., 34 (2015), pp. 191:1–191:10, https://doi.org/10.1145/2816795.2818098.

[31] A. Naitsat, E. Saucan, and Y. Y. Zeevi, *Volumetric quasi-conformal mappings - quasi-conformal mappings for volume deformation with applications to geometric modeling*, in Proceedings of the 10th International Conference on Computer Graphics Theory and Applications - Volume 1: GRAPP, (VISIGRAPP 2015), INSTICC, SciTePress, 2015, pp. 46–57, https://doi.org/10.5220/0005298900460057.

[32] G.-P. Paillé and P. Poulin, *As-conformal-as-possible discrete volumetric mapping*, Computers & Graphics, 36 (2012), pp. 427–433, https://doi.org/10.1016/j.cag.2012.03.014. Shape Modeling International (SMI) Conference 2012.

[33] G.-P. Paillé, N. Ray, P. Poulin, A. Sheffer, and B. Lévy, *Dihedral angle-based maps of tetrahedral meshes*, ACM Trans. Graph., 34 (2015), pp. 54:1–54:10, https://doi.org/10.1145/2766900.

[34] M. Rabinovich, R. Poranne, D. Panozzo, and O. Sorkine-Hornung, *Scalable locally injective mappings*, ACM Trans. Graphics, 36 (2017), pp. 16:1–16:16, https://doi.org/10.1145/2983621.

[35] R. Sawhney and K. Crane, *Boundary first flattening*, ACM Trans. Graph., 37 (2017), pp. 5:1–5:14, https://doi.org/10.1145/3132705.

[36] J. Smith and S. Schaefer, *Bijective parameterization with free boundaries*, ACM Trans. Graph., 34 (2015), pp. 70:1–70:9, https://doi.org/10.1145/2766947.

[37] K. Su, W. Chen, N. Lei, J. Zhang, K. Qian, and X. Gu, *Volume preserving mesh parameterization based on optimal mass transportation*, Comput. Aided Design, 82 (2017), pp. 42–56, https://doi.org/10.1016/j.cad.2016.05.020.

[38] K. Su, L. Cui, K. Qian, N. Lei, J. Zhang, M. Zhang, and X. D. Gu, *Area-preserving mesh parameterization for poly-annulus surfaces based on optimal mass transportation*, Comput. Aided Geom. D., 46 (2016), pp. 76–91, https://doi.org/10.1016/j.cagd.2016.05.005.

[39] J. M. Sullivan, *Conformal tiling on a torus*, in Proceedings of Bridges 2011: Mathematics, Music, Art, Architecture, Culture, 2011, pp. 593–596.

[40] Y. Tong, S. Lombeyda, A. N. Hirani, and M. Desbrun, *Discrete multiscale vector field decomposition*, ACM Trans. Graph., 22 (2003), pp. 445–452, https://doi.org/10.1145/882262.882290.

[41] Y. Wang, X. Gu, T. F. Chan, P. M. Thompson, and S.-T. Yau, *Volumetric harmonic brain mapping*, in 2004 2nd IEEE International Symposium on Biomedical Imaging: Nano to Macro (IEEE Cat No. 04EX821), vol. 2, April 2004, pp. 1275–1278, https://doi.org/10.1109/ISBI.2004.1398778.

[42] Y. Wang, X. Gu, and S.-T. Yau, *Volumetric harmonic map*, Commun. Inf. Syst., 3 (2004), pp. 191–202, https://projecteuclid.org:443/euclid.cis/1088692283.

[43] Z. Wang, Z.-x. Luo, J.-l. Zhang, and E. Saucan, *Arap++: an extension of the local/global approach to mesh parameterization*, Frontiers of Information Technology & Electronic Engineering, 17 (2016), pp. 501–515, https://doi.org/10.1631/FITEE.1500184.

[44] M.-H. Yueh, X. D. Gu, W.-W. Lin, C.-T. Wu, and S.-T. Yau, *Conformal surface registration with applications on face morphing*, 2016, http://archive.ymsc.tsinghua.edu.cn/pacm_paperurl/20160520142138341876035. mathscidoc:1605.09001.

[45] M.-H. Yueh, T. Li, W.-W. Lin, and S.-T. Yau, *A novel algorithm for volume-preserving parameterizations of 3-manifolds*, SIAM J. Imag. Sci., 12 (2019), pp. 1071–1098, https://doi.org/10.1137/18M1201184.

[46] M.-H. Yueh, W.-W. Lin, C.-T. Wu, and S.-T. Yau, *An efficient energy minimization for conformal pa-*

rameterizations, J. Sci. Comput., 73 (2017), pp. 203–227, https://doi.org/10.1007/s10915-017-0414-y.

[47] M.-H. Yueh, W.-W. Lin, C.-T. Wu, and S.-T. Yau, *A novel stretch energy minimization algorithm for equiareal parameterizations*, J. Sci. Comput., 78 (2019), pp. 1353–1386, https://doi.org/10.1007/s10915-018-0822-7.

[48] M. Zhang, R. Guo, W. Zeng, F. Luo, S.-T. Yau, and X. Gu, *The unified discrete surface ricci flow*, Graphical Models, 76 (2014), pp. 321–339, https://doi.org/10.1016/j.gmod.2014.04.008. Geometric Modeling and Processing 2014.

[49] X. Zhao, Z. Su, X. D. Gu, A. Kaufman, J. Sun, J. Gao, and F. Luo, *Area-preservation mapping using optimal mass transport*, IEEE Trans. Visual Comput. Graphics, 19 (2013), pp. 2838–2847, https://doi.org/10.1109/TVCG.2013.135.